# MEMS Platforms for *in-situ* Testing of Mechanical Properties of Nanostructures

**Yong Zhu,** Department of Mechanical and Aerospace Engineering, North Carolina State University, Raleigh, NC, United States



This is an update of R. Ballarini, H. Kahn, A.H. Heuer, M.P. De Boer, M.T. Dugger, 8.09 - MEMS Structures for On-chip Testing of Mechanical and Surface Properties of Thin Films edited by I. Milne, R.O. Ritchie, B. Karihaloo, Comprehensive Structural Integrity, Pergamon, 2003.

**Introduction** 1
**Overview** 2
Device Types and Configurations 2
Sample Preparation 3
**Nanomechanical Testing Results** 4
Quasi-Static Tensile Testing 5
Elasticity 5
Plasticity 6
Fracture 7
High Strain-Rate Testing 8
Creep and Stress Relaxation 9
Fatigue Testing 11
Thermomechanical Testing 13
Electromechanical Testing 15
**Summary and Outlook** 16
**Acknowledgment** 16
**References** 17

## Abstract

Microelectromechanical systems (MEMS) have received much interests for in-situ mechanical testing of nanostructures. This article reviews the recent advances in this promising field. MEMS platforms have been used for quasi-static tensile testing, high-strain-rate testing, true displacement- or force-controlled testing via feedback control, fatigue testing, thermomechanical testing, and multiphysical testing of nanostructures. Representative MEMS platforms and related in-situ mechanical testing of nanostructures are presented. A brief summary and outlook for future research directions are provided.

### Key Points

- Presented major types and configurations of MEMS platforms.
- Reviewed MEMS platforms for quasi-static tensile testing, high-strain-rate testing, true displacement- or force-controlled testing via feedback control, fatigue testing, thermomechanical testing, and multiphysical testing of nanostructures.
- Summarized the mechanical properties and deformation mechanisms obtained using the MEMS platforms.
- Discussed the challenges and potential directions for MEMS platforms for in-situ nanomechanical testing.

## Introduction

In this article we describe recent progress in the development of microelectromechanical system (MEMS) platforms for in-situ testing of the mechanical properties of nanostructures. Our goal is to demonstrate that the MEMS platforms can be very useful for evaluating a wide range of mechanical properties of different types of nanostructures. With the advance in nanotechnology has come a host of nanostructures, such as nanoparticles, nanowires (NWs), nanotubes and 2D materials (e.g., graphene, hexagonal boron nitride, and transition metal dichalcogenides) that exhibit outstanding mechanical properties. Such nanostructures are important building blocks for a broad spectrum of applications including energy harvesting and storage (Chan *et al.*, 2008; Liu *et al.*, 2012; Wang and Song, 2006), nanoelectromechanical systems (NEMS) (Feng *et al.*, 2007; Loh and Espinosa, 2012), flexible electronics (Fan *et al.*, 2009; McAlpine *et al.*, 2003) and stretchable electronics (Kim *et al.*, 2009; Lipomi *et al.*, 2011; Ryu *et al.*, 2009; Xu *et al.*, 2011; Yao and Zhu, 2015), where their mechanical properties are of significant relevance.

These nanostructures can provide valuable insights into fundamental deformation mechanisms owing to their small size (typically around 100 nm or less) and scarce and often well-defined defect structures. With the small size, on one hand, they are compatible with transmission electron microscopy observation without additional sample preparation; on the other hand, they come increasingly within the reach of the state-of-the-art computational modeling capabilities, thus making possible direct comparison between nanomechanical tests and atomistic simulations. As a result of the "bottom-up" synthesis, nanostructures typically possess few defects and the defects can be well characterized. Recent advances in nanomechanical testing methods (Agrawal *et al.*, 2011; Gianola and Eberl, 2009; Kang *et al.*, 2017; Zhu, 2016; Zhu *et al.*, 2007) and imaging tools such as electron microscopies (Minor and Dehm, 2019; Robertson *et al.*, 2011, 2008) has enabled real-time observation of deformation and defect dynamics. For example, dislocation nucleation from free surfaces has been found as the dominant dislocation mechanism at the nanoscale (Diao *et al.*, 2003; Park and Zimmerman, 2005; Zheng *et al.*, 2010; Zhu *et al.*, 2008). Dislocation-twin boundary (TB) interactions have been found responsible for interesting mechanical behaviors such as recoverable plasticity (Qin *et al.*, 2015), Bauschinger effect (Bernal *et al.*, 2015), and detwinning under nominally tensile loading (Cheng *et al.*, 2017). In addition, the nanostructures can serve as model systems to probe critical mechanical behaviors. For example, metal NWs have been used to investigate hydrogen embrittlement, unambiguously showing that hydrogen near the NW surface can suppress surface dislocation nucleation, resulting in reduced plastic deformation (Yin *et al.*, 2019a).

The article is organized as follows. In Section "Overview", We start with three commonly used device types, based on the involvement of external and/or on-chip transducers, and related device configurations and other considerations such as sample preparation. Other relevant issues such as device fabrication and displacement/strain measurements are not covered. Interested readers are referred to previous reviews (Haque *et al.*, 2011; Zhu and Chang, 2015). In Section "Nanomechanical Testing Results", representative MEMS platforms and testing results inside electron microscopy such as scanning and transmission electron microscopy (SEM/TEM) are reviewed. Such platforms have been used for quasi-static tensile testing, high-strain-rate testing, true displacement- or force-controlled testing via feedback control, fatigue testing, thermomechanical testing, and multiphysical testing of nanostructures. Finally, some of the challenges and future directions in the area of MEMS-enabled nanomechanical testing are discussed.

## Overview

In this section, we present three common device types for tensile testing along with typical MEMS actuation and sensing methods used in the testing. Next, a brief review of the manipulation methods to mount nanostructures onto the MEMS platforms is presented. In this review, we limit the scope to uniaxial tensile testing, although the MEMS devices can be readily applied for compression (Espinosa *et al.*, 2007) and bending (Kang and Saif, 2013) testing too.

### Device Types and Configurations

Tensile test is the most straightforward testing method to measure mechanical properties. In bulk a tensile testing machine typically consists of three parts: an actuator, a load cell (sensor), and a pair of grips for mounting specimens. The same concept is applied at the small scale. There have been considerable efforts in developing instrumentation for micro/nano-scale tensile testing. However, the methods for actuation, load sensing and sample gripping are different from and often much more difficult than the large-scale ones. MEMS-based actuation and load sensing have received much interests recently. MEMS devices can be categorized into three types, based on the involvement of external and/or on-chip transducers. The first type employs external actuation and load sensing, the second type does external actuation but on-chip load sensing, and the third type does on-chip actuation and load sensing. For all three types, the testing platform is microfabricated, while the specimen is either co-fabricated with or later mounted onto the testing platform.

For the first type, an existing transducer (e.g., nanoindenter) that includes both actuation and load sensing is typically used. A widely used device configuration is based on the so-called "push-to-pull" concept, where a microfabricated structure that can convert compression from the transducer to tension on the specimen. **Fig. 1**(a) shows a push-to-pull platform that can be used together with a TEM nanoindentation holder to perform in-situ TEM tensile testing (Guo *et al.*, 2011; Oh *et al.*, 2010). The stage consists of a fixed part and a freestanding part that is supported by four folded beams. When an indenter head pushes the freestanding part, the gap between the fixed and freestanding parts expands, applying a tensile load to the specimen that is bridged across the gap. The force and displacement of the specimen are derived from the nanoindenter signals; it is critical to calibrate the elastic response of the push-to-push structure *a prior*. The push-to-pull concept has also been used in other MEMS structures, e.g., a Theta-like structure (Durelli *et al.*, 1962; Gaither *et al.*, 2011), for tensile testing of nanostructures (Ganesan *et al.*, 2010; Lu *et al.*, 2011a,b; Zhang *et al.*, 2014).

For the second (hybrid) type, Haque and Saif pioneered developing a MEMS platform for tensile testing of metallic thin films (Haque and Saif, 2004, 2002a,b). The MEMS platform is stretched by an external actuator (e.g., a piezoelectric actuator available in a conventional TEM straining holder). U-shaped beams are designed to guide the alignment of the applied force along the specimen axial direction. The external actuator can be either hooked (Samuel *et al.*, 2007) or glued (Naraghi *et al.*, 2007a) to the gripping pad to impose the displacement. The specimen is located between the external actuator and a microfabricated load sensor beam; the force is obtained by measuring the deflection of the load sensor beam, while the displacement is obtained by tracking two fiducial markers on both sides of the specimen. The thin film specimen is co-fabricated with the MEMS stage.

For the third (on-chip) type, electrostatic and thermal actuation are the two most popular actuation mechanisms due to their compatibility with typical microfabrication processes (Espinosa *et al.*, 2007; Zhu *et al.*, 2005). For electrostatic actuation, the comb-

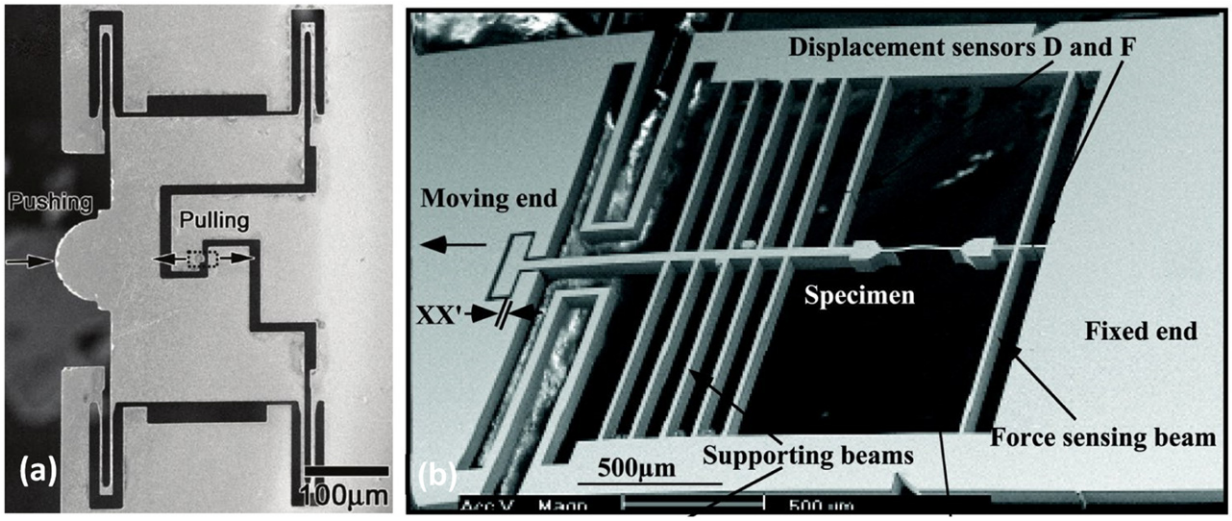


**Fig. 1** (a) The first type of MEMS platform using the push-to-pull concept. (b) The second type of MEMS platform using an external piezo actuator and an on-chip force sensing beam.

drive actuator is widely used as the generated electrostatic force is nearly constant over the travel range at a given voltage (Saif and MacDonald, 1996). Thermal actuation is based on Joule heating; so-called V-shaped (Que *et al.*, 2001; Zhu *et al.*, 2006) and Z-shaped thermal actuators (Guan and Zhu, 2010a; Ouyang and Zhu, 2012) are most widely used. A critical challenge for using thermal actuators in nanomechanical testing is the undesired heating of the specimen. To mitigate this problem, Zhu *et al.* introduced a heat sink mechanism between the actuator and the specimen, which can limit the temperature rise at the specimen region to below 5°C without adding extra steps in microfabrication to introduce the heat sink structure (Qin and Zhu, 2013; Zhu *et al.*, 2006).

For both the second and third types, an on-chip load sensor is typically made of a flexible member, so the force is measured as the sensor displacement multiplied by the sensor stiffness. In addition to direct imaging of the sensor displacement, electronic sensing can be realized using a few mechanisms including capacitive sensing and piezoresistive sensing. Capacitive sensing is perhaps the most popular sensing mechanism in MEMS with commercially available chips for data acquisition. In particular, differential capacitive sensing has been widely used in many MEMS devices such as accelerometers (Boser and Howe, 1996). Several authors have incorporated a commercially available sensing chip (MS3110, MicroSensors) in their MEMS platforms with a differential capacitive sensor (Pant *et al.*, 2011; Zhang *et al.*, 2009b; Zhu and Espinosa, 2005). Si is a common piezoresistive material including single-crystalline and polycrystalline Si, therefore piezoresistive sensing is widely used in MEMS (Barlian *et al.*, 2009; Messenger *et al.*, 2009) and has been recently explored for load sensing in MEMS testing platforms (Ouyang and Zhu, 2012).

The on-chip MEMS platforms include two typical configurations, depending on the relative position of the specimen. In the first configuration the specimen is positioned between the actuator and the load sensor (**Fig. 2**(a) and (b)) (Zhu *et al.*, 2005; Zhu and Espinosa, 2005), while in the second the load sensor is between the actuator and the specimen (**Fig. 2**(c)) (Li *et al.*, 2020a,b). The first configuration is more commonly used (Chen *et al.*, 2012; Pant *et al.*, 2011; Steighner *et al.*, 2011; Zhang *et al.*, 2009b), e.g., also used in the externally actuated platform by Haque and Saif (2002a). But one drawback is that the specimen moves a lot due to the rigid-body motion as a result of the load sensor displacement, which could add challenges for in-situ observations. The second configuration can overcome this drawback as one end of the specimen is fixed (Tsuchiya *et al.*, 2012). As shown in **Fig. 2**(c), the specimen displacement is measured by sensor B, while the load is measured by the displacement difference between sensors A and B multiplied by the load cell (sensor) stiffness. Note that the load cell is a simple folded beam.

For the three types of MEMS platforms, we only discussed the basic capabilities for quasi-static tensile testing. But these platforms offer tremendous potential for further developments to meet advanced testing needs such as high strain rate, fatigue, displacement control, creep and stress relaxation, thermomechanical testing, and electromechanical testing, especially using the on-chip type. In Section "Nano-mechanical Testing Results" we will discuss the results obtained from these advanced testing capabilities after the basic testing capabilities.

## Sample Preparation

A key step is to integrate the nano-specimen onto the MEMS platform with the specimen aligned with the loading direction and clamped at both ends. Two major methods are used, co-fabrication of the specimen with the device and "pick-and-place" by nanomanipulation (Zhu and Espinosa, 2005). Here we briefly discuss these sample preparation methods, while more details can be found elsewhere (Espinosa *et al.*, 2012; Zhu *et al.*, 2007).

A flexible and widely used method for mounting "bottom-up" synthesized nanostructures onto MEMS devices is "pick-and-place" by nanomanipulation (Zhu and Espinosa, 2005). Electron Beam Induced Deposition (EBID) of residual hydrocarbon in a SEM chamber or a precursor gas (e.g., platinum) is commonly used for clamping the samples. This method has been used successfully for

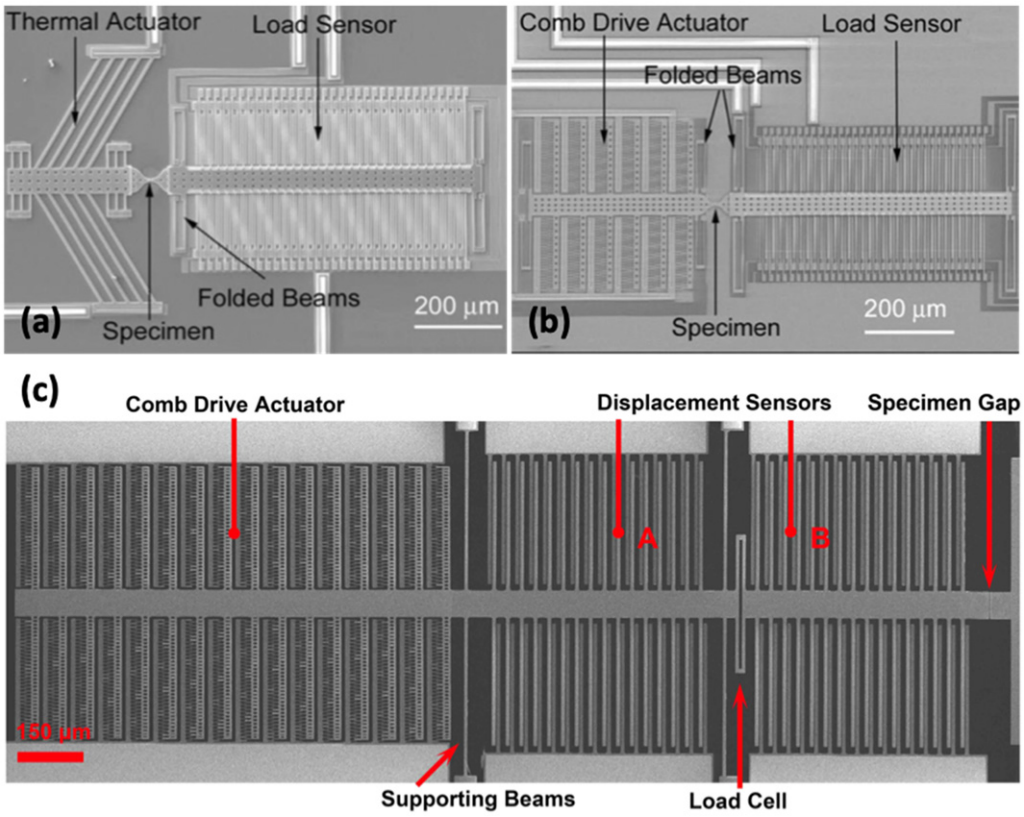


**Fig. 2** The third type of MEMS platform with two configurations. In the first configuration the specimen is positioned between the actuator, either thermal actuator (a) or comb drive actuator (b), and the load sensor; (c) in the second configuration the load sensor is between the actuator and the specimen. Reproduced from Zhu, Y., Moldovan, N., Espinosa, H.D., 2005. A microelectromechanical load sensor for in situ electron and x-ray microscopy tensile testing of nanostructures. Appl. Phys. Lett. 86, 13506. Li, C., Cheng, G., Wang, H., Zhu, Y., 2020a. Microelectromechanical systems for nanomechanical testing: Displacement- and force-controlled tensile testing with feedback control. Exp. Mech. 60, 1005–1015. Available at: https://doi.org/10.1007/s11340-020-00619-z.

a wide range of nano-structures (Agrawal *et al.*, 2009; Chen *et al.*, 2012; Guo *et al.*, 2011; Peng *et al.*, 2008; Zhang *et al.*, 2009a; Zhang *et al.*, 2011; Zhu *et al.*, 2009). However, the process is labor intensive. And it is unclear if the clamping mechanism is sufficiently rigid and strong. Gianola and co-workers reported specimen sliding due to compliance and permanent deformation of the clamps (Murphy *et al.*, 2013). Zhu and co-workers found that the measured Young's modulus of a NW (using the resonance method) depends on the clamping. They pointed out true Young's modulus can be measured if the critical clamp size is reached. The critical clamp size is a function of the NW diameter and modulus ratio of the clamp material and the NW. Adhesives (e.g., epoxy) have been used to clamp polymer nanofibers (Naraghi *et al.*, 2007b), carbon nanotubes (Ganesan *et al.*, 2010) and Ni nanobeams (Hosseinian and Pierron, 2013). For larger specimens, e.g., thin films, separately fabricated samples can be mounted onto a MEMS device with pre-patterned grips using the "pick-and-place" approach (Kang *et al.*, 2010; Liebig *et al.*, 2016).

Co-fabrication is a more scalable method to integrate the "top-down" specimens during the microfabrication process. However, the fabrication process is typically more complicated and the materials that can be co-fabricated are limited. Several groups have developed specialized fabrication processes to incorporate Au NWs (Yilmaz and Kysar, 2013), Al films (Han and Saif, 2006; Haque and Saif, 2002b), Au films (Rajagopalan *et al.*, 2007), and Pt ultra-thin films (Abbas *et al.*, 2012) onto the MEMS devices for in situ tensile testing. Due to the residual stresses involved in the fabrication processes, the specimens can be stressed after fabrication, e.g., buckled.

An extension of the co-fabrication method is directed synthesis, that is, "bottom-up" synthesis of nanostructures into "top-down" fabricated MEMS devices. This is a promising method that can be more scalable than the "pick-and-place" approach. The boundary conditions are also supposed to be more robust. However, so far only limited materials have been synthesized, including Si (He and Yang, 2006) and Ge NWs (Greil *et al.*, 2012) between microfabricated Si posts. Moreover, no direct synthesis into movable MEMS devices has been reported.

## Nanomechanical Testing Results

A wide range of nanostructures have been tested using MEMS platforms (Agrawal *et al.*, 2009, 2008; Bernal *et al.*, 2015, 2011; Brown *et al.*, 2011, 2009; Chang and Zhu, 2013; Chen *et al.*, 2012, 2015; Cheng *et al.*, 2019, 2017, 2014, 2020; Chisholm *et al.*, 2012;

Desai and Haque, 2007; Filleter *et al.*, 2012; Ganesan *et al.*, 2010; Guo *et al.*, 2013, 2011; Hosseinian and Pierron, 2013; Kiuchi *et al.*, 2007; Locascio *et al.*, 2009; Lu *et al.*, 2011a; Naraghi *et al.*, 2010, 2007a,b; Ozkan *et al.*, 2010; Pant *et al.*, 2012, 2011; Peng *et al.*, 2008, 2012; Qin *et al.*, 2015; Ramachandramoorthy *et al.*, 2017, 2016; Steighner *et al.*, 2011; Tsuchiya *et al.*, 2012, 2008; Yashinski and Muhlstein, 2013; Yilmaz and Kysar, 2013; Yin *et al.*, 2019a,b; Zhang *et al.*, 2009a; Zhang *et al.*, 2010, 2011, 2016; Zhu and Espinosa, 2005). Here we only discuss representative results to highlight the testing capabilities of the MEMS platforms.

## Quasi-Static Tensile Testing

Key mechanical properties can be obtained from quasi-static tensile tests including elasticity (Young's modulus), plasticity, and fracture. For nanostructures especially NWs, such tests have enabled the study on size effect on these mechanical properties in addition to the deformation mechanisms.

### *Elasticity*

Size effect in elasticity is in general originated from surface elasticity (i.e., surface atoms can be stiffer or softer than the bulk atoms) and surface stress (Zhou and Huang, 2004). The softening effect is primarily due to the bond loss (i.e., loss of neighboring atoms on the surface), while the stiffening effect can be attributed to the electron redistribution (often called bond saturation) (Shim *et al.*, 2005; Zhou and Huang, 2004) and/or surface reconstruction (Agrawal *et al.*, 2008; Shim *et al.*, 2005). Another mechanism that contributes to the size effect in elasticity is so-called bulk nonlinear elasticity. The compressive stress in the interior of a nanostructure caused by the tensile surface stress, notably in metallic nanostructures, is large enough to induce a nonlinear increase in the Young's modulus of the interior atoms (Liang *et al.*, 2005).

Agrawal *et al.* (2008) performed in-situ TEM tensile tests on [0001]-oriented ZnO NWs using a MEMS testing platform. A pronounced size effect in elasticity was found; more specifically, the Young's modulus increases as the NW diameter decreases below ~80 nm while remains close to the bulk value (140 GPa) for NWs with larger diameters. Molecular dynamics (MD) simulations found that the surface atoms significantly contract towards the NW interior during surface reconstruction, leading to overall smaller interatomic spacing near the surface and hence stronger Coulomb force, which is responsible for the observed stiffening size effect in elasticity. Other studies using the resonance test (Chen *et al.*, 2006) and the tension and buckling tests (Xu *et al.*, 2010) also reported the similar stiffening size effect in ZnO NWs. Other NWs of ionic bonding (e.g., GaN NWs) exhibited a similar stiffening size effect, though much smaller in magnitude than ZnO NWs (Bernal *et al.*, 2011).

NWs of covalent bonding and metallic bonding also exhibit size effects in elasticity but with different trends. In the case of Si NWs, Zhu *et al.* (2009) reported a softening size effect – the Young's modulus decreases with the decreasing diameters when the diameter is below about 30 nm – which was attributed to the bond loss. In the case of penta-twinned Ag NWs, Zhu *et al.* (2012) and Filleter *et al.* (2012) reported pronounced stiffening effect, i.e., an increase of Young's modulus with decreasing NW diameter. The penta-twinned Ag NWs were synthesized by the polyol method with <110> axial orientation and five {100} side surfaces (Sun and Xia, 2002). Note that a penta-twinned NW has five twin segments joined along a common quintuple line in the axial direction. Two independent tests on the same NW, in situ scanning electron microscopy (SEM) resonance test and tensile test, were conducted to further understand the size effect in elasticity in Ag NWs (Chang *et al.*, 2016). **Fig. 3** shows the size effect in Young's modulus under the two types of the tests, considering the size-dependent cross-sectional shape (to be discussed in the following). A comparison of the measured Young's moduli under the two types of tests suggested that some combination of bulk nonlinear elasticity and surface elasticity is responsible for the observed elasticity size effect in Ag NWs.

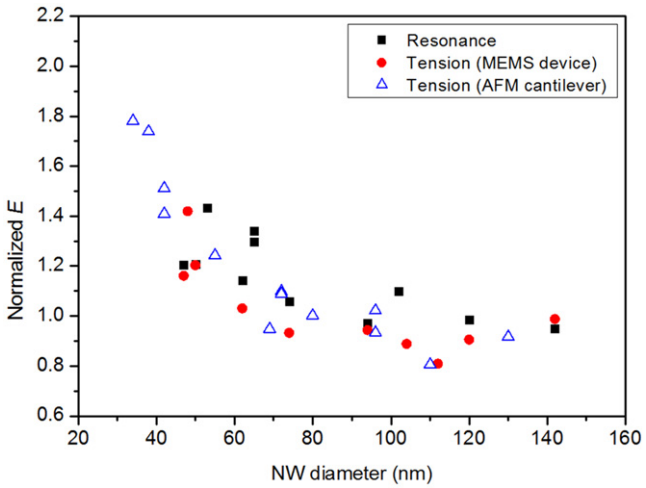


**Fig. 3** Young's modulus as a function of Ag NW diameter. The measured Young's modulus was normalized by the bulk modulus of 84 GPa. Reproduced from Chang, T.-H., Cheng, G., Li, C., Zhu, Y., 2016. On the size-dependent elasticity of penta-twinned silver nanowires. Extreme Mech. Lett. 8, 177–183. Available at: https://doi.org/10.1016/j.eml.2016.03.007.

In addition to the clamping effect mentioned in Section "Sample Preparation", two other effects are important in measuring mechanical properties of NWs especially elasticity. The first is the effect of cross section. NWs typically possess well-defined facets with side surfaces of low surface energy, e.g., truncated rhombic cross section with {111} and {110} side surfaces for metal NWs (Yin *et al.*, 2019b). It is important to know the cross-sectional shape when calculating the stress (tension test) or resonance frequency (resonance test), rather than simply assuming the circular cross section. Indeed, the NW cross section could with the diameter. For example, the cross-sectional shape of the Ag NWs was found to transit from pentagon to circle with decreasing NW diameter, which can modify the Young's modulus as much as 8% (for resonance test) and 19% (for tensile test) for the tested diameter range (30–140 nm) (Chang *et al.*, 2016). The second is the effect of anisotropic elasticity. Crystalline NWs are typically anisotropic, however, we usually assume isotropy (e.g., when calculating the resonance frequency in the resonance test). The anisotropic elasticity effect was found negligible for a cantilevered NW (Chang *et al.*, 2016), especially under two conditions: (1) the length to diameter ratio (aspect ratio) is over 10 and (2) the resonance amplitude is below a certain fraction of the NW length (e.g., $< L/10$).

### Plasticity

It is now well known that surface dislocation nucleation plays a dominant role in the incipient plasticity of metallic NWs (Diao *et al.*, 2003; Park and Zimmerman, 2005; Zheng *et al.*, 2010; Zhu *et al.*, 2008). Following the incipient plasticity, twining and dislocation slip are two competitive deformation mechanisms in face-centered cubic (FCC) metals. The rivalry between the two mechanisms prevails in FCC metallic NWs, depending on the axial orientation (Schmid factor) and the generalized stacking fault energies (Weinberger and Cai, 2012). In NWs both mechanisms start with partial dislocation nucleation from the free surfaces. Yin *et al.* (2019b) recently found that another factor, cross-sectional shape, can influence the competition between the two mechanisms in single-crystalline Ag NWs using in-situ TEM tensile testing and MD simulations, as shown in **Fig. 4**. The single-crystalline Ag NWs were synthesized by using a high-temperature molecular beam epitaxy method (Richter *et al.*, 2009). Twin deformation accompanied by a large plasticity occurred in NWs with low aspect ratios. With the increasing aspect ratio, a shift in deformation mode from twinning to dislocation slip was observed. It was found that the energy barrier for twinning depends on the aspect ratio of the cross section, proportional to the change in surface energy caused by the twinning-induced reorientation of the surface facets.

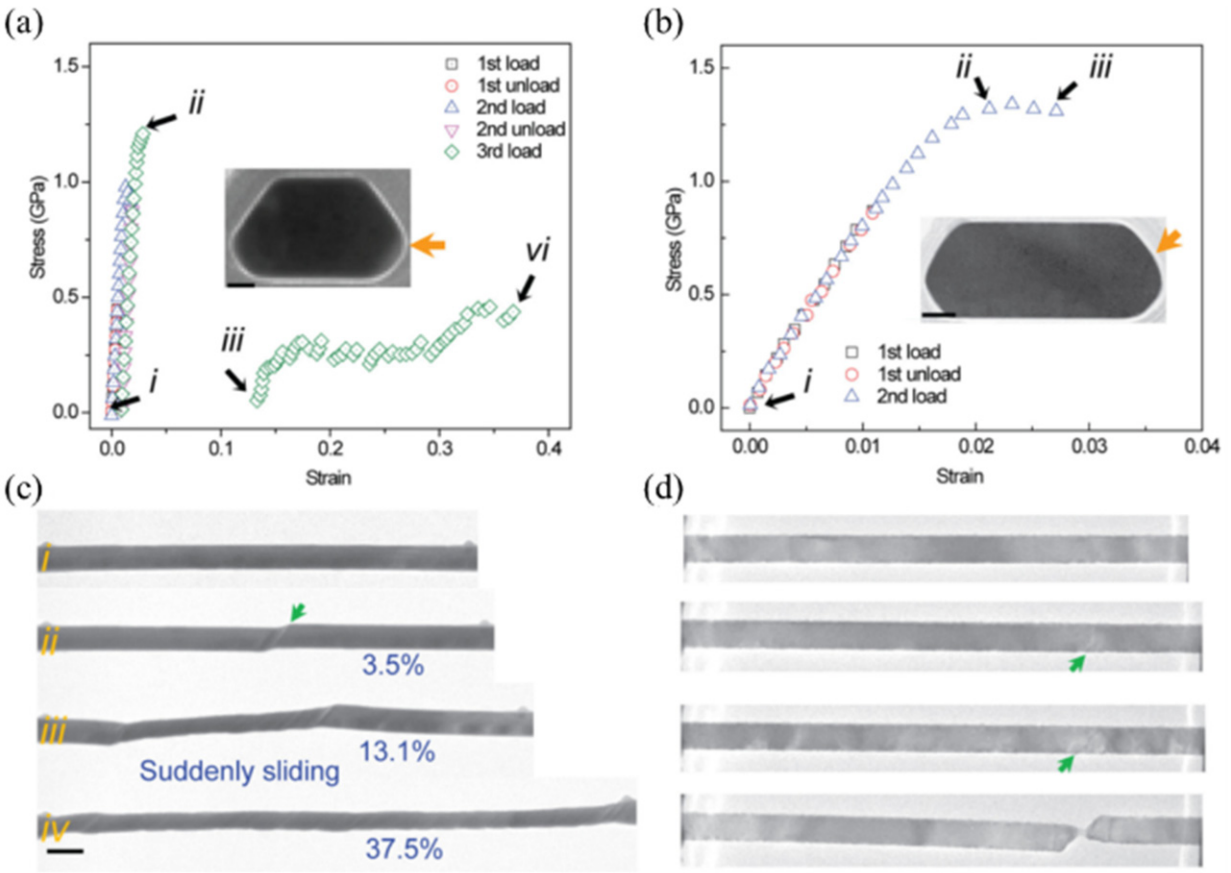


**Fig. 4** Engineering stress–strain curves of two single-crystalline Ag NWs with different aspect ratios, (a, c) small aspect ratio, (b, d) large aspect ratio. Reproduced from Yin, S., Cheng, G., Richter, G., Gao, H., Zhu, Y., 2019b. Transition of deformation mechanisms in single-crystalline metallic nanowires. ACS Nano 13, 9082–9090. Available at: https://doi.org/10.1021/acsnano.9b03311.

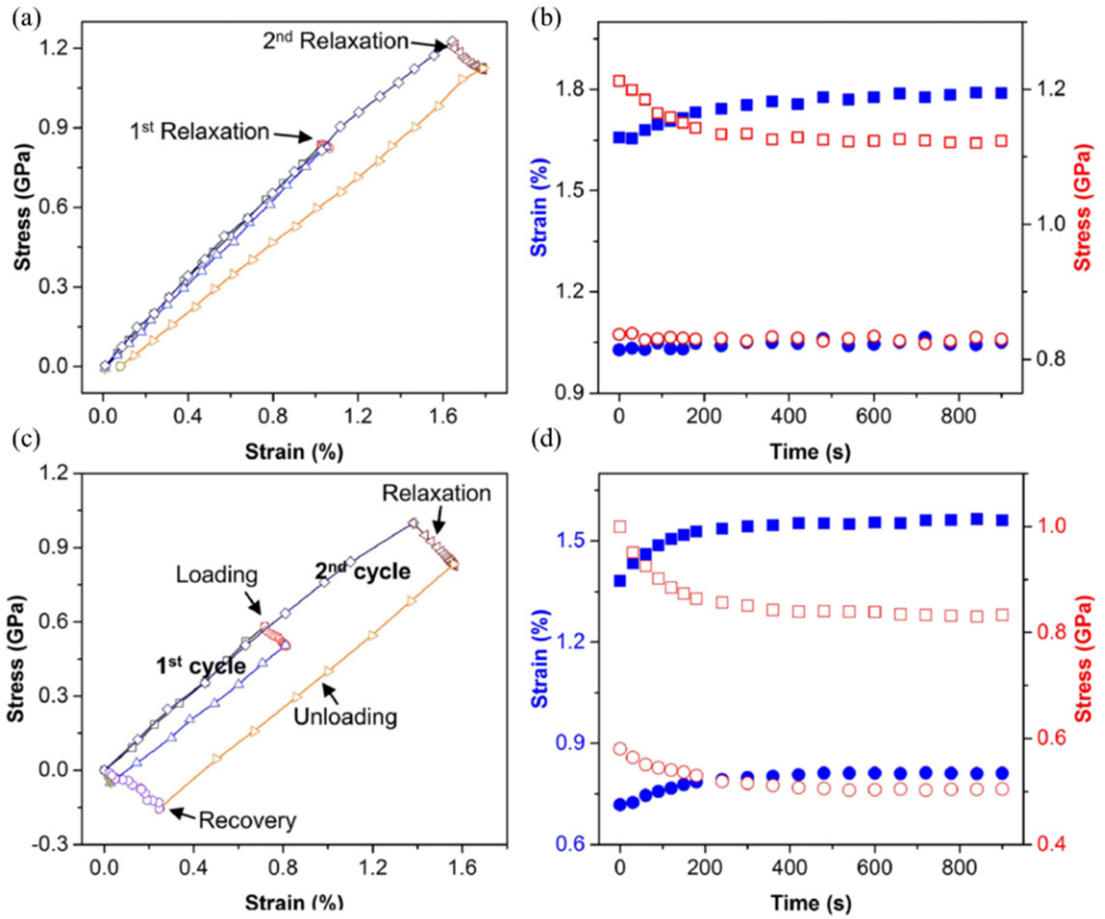


**Fig. 5** In-situ measurements of stress and strain evolutions in bi- (a,b) and penta-twinned (c,d) Ag NWs. (a,c) Stress–strain curves for the bi- and penta-twinned NWs under two cycles of loading-relaxation-unloading-recovery, respectively. The relaxation and recovery steps took 15 min (b,d) Relaxation curves for the bi- and penta-twinned NWs, respectively. Solid and open symbols correspond to the strain-time and stress-time relationships, respectively. Square and circle symbols to high and low initial stress levels, respectively. Reproduced from Cheng, G., Yin, S., Li, C., *et al.*, 2020. In-situ TEM study of dislocation interaction with twin boundary and retraction in twinned metallic nanowires. Acta Mater. 196, 304–312. Available at: https://doi.org/10.1016/j.actamat.2020.06.055. https://doi.org/10.1016/j.actamat.2020.06.055. Qin, Q., Yin, S., Cheng, G., *et al.*, 2015. Recoverable plasticity in penta-twinned metallic nanowires governed by dislocation nucleation and retraction. Nat. Commun. 6, 5983. Available at: https://doi.org/10.1038/ncomms6983.

For NWs containing internal TBs, dislocations nucleated from free surfaces interact with TBs, leading to interesting mechanical behaviors such as recoverable plasticity and strain hardening. In the case of bi-twinned Ag NWs with a single TB parallel to the NW axis, partial dislocations can be hindered by the TB, and upon unloading all or part of the partial dislocations retract from the TB, leading to full or partial plastic strain recovery, respectively (**Fig. 5**(a)) (Cheng *et al.*, 2020). The bi-twinned Ag NWs can also undergo stress relaxation, as a result of dislocation nucleation (**Fig. 5**(b)) (Cheng *et al.*, 2020). Under larger loading, the partial dislocations can transmit across the TB, leading to localized dislocation slip or necking and eventual fracture. However, when the volume ratio between the two twin variants is small, another deformation mechanism – detwinning of the existing TB – could occur (Cheng *et al.*, 2017), which can result in the twinning behavior similar to that reported in single-crystalline Ag NWs (Yin *et al.*, 2019b).

For penta-twinned Ag NWs, stress relaxation and plastic strain recovery were also observed, similar to the bi-twinned Ag NWs but to a larger extent (**Fig. 5**(c) and (d)). The inhomogeneous stress field generated intrinsically by the fivefold twin structure can further drive the partial dislocations back upon unloading (Bernal *et al.*, 2015; Qin *et al.*, 2015). The TBs confine dislocation activities with a direct impact on ductility and strength by forming a complicated 3D dislocation structure (Filleter *et al.*, 2012; Narayanan *et al.*, 2015). MEMS-based tensile testing was used to study the influence of strain rate on the deformation of Ag NWs. Brittle fracture was observed at low strain rates, while ductile fracture at high strain rates (Ramachandramoorthy *et al.*, 2016).

### *Fracture*

Mechanical properties of SiC NWs have been measured via in situ SEM tensile tests using a MEMS platform (Cheng *et al.*, 2014), where internal defects, stacking faults, were found to play a critical role. The SiC NWs with the $< 111 >$ axial orientation were synthesized by the CVD-VLS process (Shim and Huang, 2007). The microstructure of SiC NWs consisted of pure 3C structure, 3C

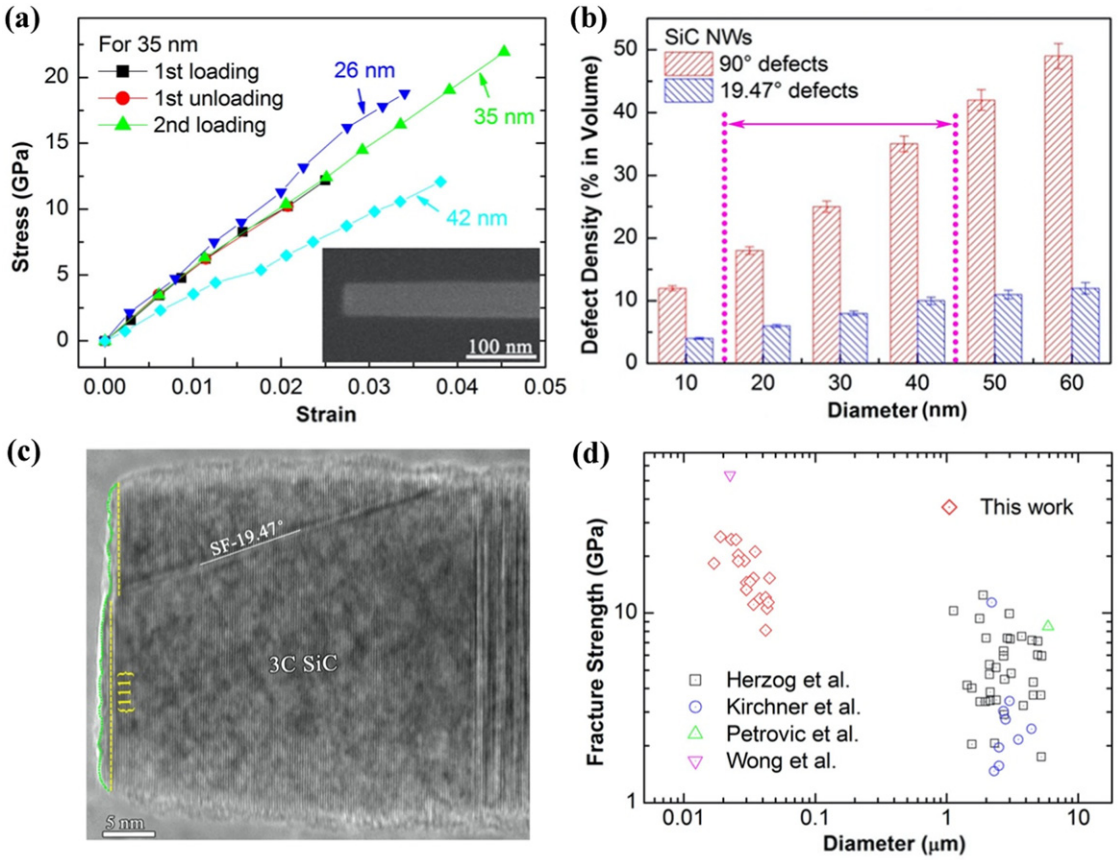


**Fig. 6** (a) Representative tensile stress – strain curves of SiC NWs. (b) Defect density as a function of NW diameter. Here 90° and 19.47° defects refer to highly defective structures and 3C structures with a 19.47° SFs, respectively. (c) High-resolution TEM image of the fracture surface of a SiC NW. (d) Fracture strength of SiC NWs and whiskers as a function of the diameter. Reproduced from Cheng, G., Chang, T.-H., Qin, Q., Huang, H., Zhu, Y., 2014. Mechanical properties of silicon carbide nanowires: effect of size-dependent defect density. Nano Lett. 14, 754–758. Available at: https://doi.org/10.1021/nl404058r.

structure with an inclined stacking fault, and highly defective structure in a periodic fashion along the NW length. The SiC NWs were reported to fail in brittle fracture at room temperature, in contrast to the superplasticity reported previously (Zhang *et al.*, 2007). The SiC NWs exhibited strong size effect in the fracture strength, that is, the fracture strength increased with decreasing diameter, up to $> 25$ GPa approaching the theoretical strength of 3C SiC (**Fig. 6**(a)). The size effect on fracture strength was reported to be due to the size-dependent defect density (of the 3C structure with 19.47° stacking faults), rather than the surface effect as commonly believed (**Fig. 6**(b)). Interestingly all the cracks were initiated and propagated in the 3C segments with the 19.47° stacking faults rather than in the highly defective segments (**Fig. 6**(c)), in good agreement with MD simulations (Wang *et al.*, 2012). **Fig. 6**(d) shows the available fracture strength data of SiC NWs in the literature as a function of NW diameter.

## High Strain-Rate Testing

Nanostructures are building blocks for applications like NEMS and flexible/stretchable electronics, where the loading rate can be high. On the other hand, MD simulations of nanostructures are typically conducted at strain rates of $10^7$ to $10^9$ $s^{-1}$, which is over 10 orders of magnitude higher than the quasi-static experimental strain rates (typically $10^{-5}$ to $10^{-1}$ $s^{-1}$). Because of this mismatch, most experimental results cannot be directly compared to the MD results, hindering our understanding of the nanoscale mechanics. For these reasons it is of paramount importance to conduct nanomechanical testing at high strain rates. However, conducting such testing is challenging. Few rate-dependent experiments have been reported on nanostructures. With the electronically-controlled actuation and load sensing, MEMS based testing platforms offer a promising potential for high strain-rate nanomechanical testing.

Ramachandramoorthy *et al.* reported in-situ SEM tensile testing of bicrystalline Ag NWs at strain rates up to $2\ s^{-1}$ (Ramachandramoorthy *et al.*, 2016). A V-shaped thermal actuator was employed to provide the fast actuation. Both experiments and multiphysics simulations showed that the thermal actuator displacement remains linear up to 10 μm/s. An interesting brittle-to-ductile failure mode transition was observed at a threshold strain rate of $0.2\ s^{-1}$. TEM observation revealed that dislocation density and localized plastic regions increase with increasing strain rate (**Fig. 7**(a)-(d)). As shown in **Fig. 7**(e), up to a strain rate of 0.02/s, the NWs failed in a brittle-like fashion. At higher strain rates, a drastic increase in ductility was observed, accompanied by modest

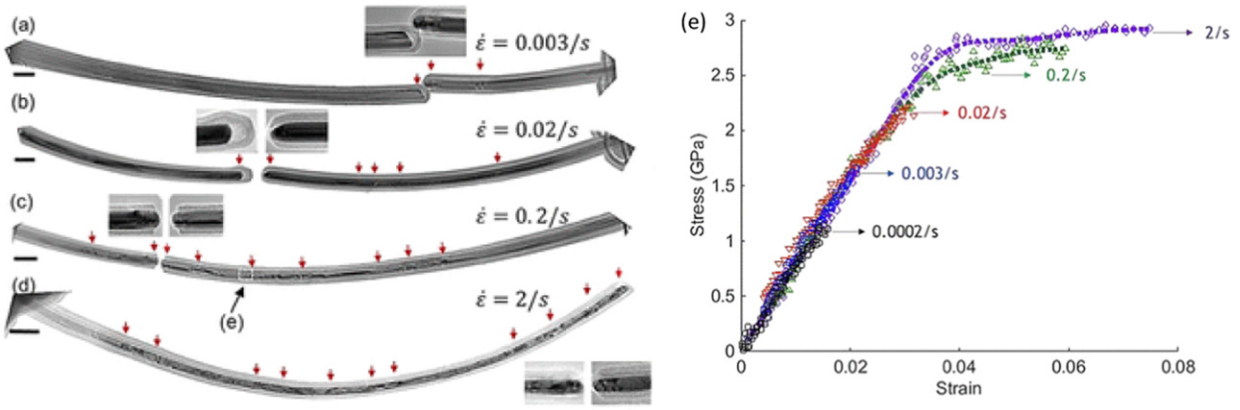


**Fig. 7** Stitched TEM images of the bicrystalline NWs tested at (a) quasistatic 0.003/s strain rate (scale bar 80 nm), (b) 0.02/s strain rate (scale bar 80 nm), (c) 0.2/s (scale bar 80 nm), and (d) 2/s (scale bar 100 nm). Red arrows point to plastic regions. Fracture surfaces with high magnifications are shown in the insets. (e) Stress–strain curves at the corresponding strain rates. Reproduced from Ramachandramoorthy, R., Gao, W., Bernal, R., Espinosa, H. 2016. High strain rate tensile testing of silver nanowires: Rate-dependent brittle-to-ductile transition. Nano Lett. 16, 255–263. https://doi.org/10.1021/ acs.nanolett.5b03630.

strain hardening. MD simulations showed that the ductility is attributed to deformation mechanisms such as grain boundary migration and dislocation interactions. This work nicely demonstrated the capability of MEMS platforms for high strain-rate nanomechanical testing as well as important mechanics insights this type of testing can offer. However, the thermal actuator is limited in the actuation speed due to the relatively slow heat transfer process involved (Guan and Zhu, 2010b; Lott *et al.*, 2002).

To further increase the actuation speed, electrostatic actuation was sought. Li *et al.* (2020b) reported a MEMS platform with an electrostatic (comb-drive) actuator that achieved a constant strain rate over 200 $s^{-1}$. An analytical model was derived to systematically investigate the dynamic response of the MEMS platform to alternating and ramp actuation forces in both vacuum and air. Two methods, capacitive readout and high-speed optical imaging, were used to measure the dynamic displacements. The natural frequencies and damping coefficients of the MEMS platform were obtained through model fitting, which were then used to predict its dynamic response under the ramp force. It was found that even under the linear ramp force (a linear function of time) the displacement is not linear, rather it includes a linear term and an oscillatory term as a result of the system dynamics. **Fig. 8** shows the displacement of the MEMS platform under a ramp force in air, using the optical imaging.

Both capacitive readout and high-speed optical imaging were used to measure the displacements. The experimental results showed good agreement with the modeling results. The maximum strain rate the device can attain was found to be about 200 $s^{-1}$. However, the capacitive readout used can only measure strain rate up to 22.6 $s^{-1}$ (gauge length 2 μm) due to its limited bandwidth, which is nevertheless an order of magnitude higher than the highest strain rate (2 $s^{-1}$) reported so far using an electronic sensor.

The MEMS platform was used to test two single-crystalline gold nanowires at strain rates of $10^{-5}$ and 10 $s^{-1}$ (Li *et al.*, 2020b). The test at 10 $s^{-1}$ exhibited enhanced ductility with a much larger fracture strain, consistent with the results by Ramachandramoorthy. In addition, a more uniform decrease in diameter occurred under the high strain rate; by contrast, necking occurred at the lower strain rate.

## Creep and Stress Relaxation

The majority of the current MEMS-based testing platforms have a common limitation, that is, they are neither truly displacement- nor force-controlled, which is necessary for capturing mechanical behaviors like stress relaxation, rapid stress drop due to certain relaxation mechanisms (e.g., dislocation or crack nucleation/propagation), creep and etc. This limitation originates from the limited stiffness of the load sensor (often comparable to or even smaller than that of the specimen); the load sensor need to deform substantially in order to detect the force, so the specimen deformation is coupled with the load sensor deformation (Espinosa *et al.*, 2007; Naraghi *et al.*, 2007a).

To address this issue, a straightforward method is to increase the stiffness of the load sensor. It did prevent catastrophic fracture in NWs, leading to the observation of stable plasticity. However, the drawback is obvious too – the force cannot be measured (Shin *et al.*, 2020). The other method is to employ electronic feedback control. Pantano *et al.* (2014) developed a feedback control scheme by adding an additional actuator at the far end of the capacitive load sensor, which can pull the load sensor back to the original position via feedback control. Using this scheme displacement-controlled loading was realized. The force in this case was measured by the feedback voltage applied to the additional actuator. While this work is an impressive advance in the field, two limitations exist: (1) an extra actuator must be added, and (2) this scheme cannot realize force-controlled loading. In addition to capacitance, other sensing mechanisms have been explored for feedback control such as piezoresistivity (Ouyang and Zhu, 2012).

Recently Zhu and co-workers have reported a MEMS-based platform using a new electronic feedback control scheme that can achieve both displacement- and force-controlled tensile testing without the need of an additional actuator (Li *et al.*, 2020a). The device was comprised of an electrostatic actuator and two capacitive sensors (**Fig. 1**(c)). Feedback control was implemented using a

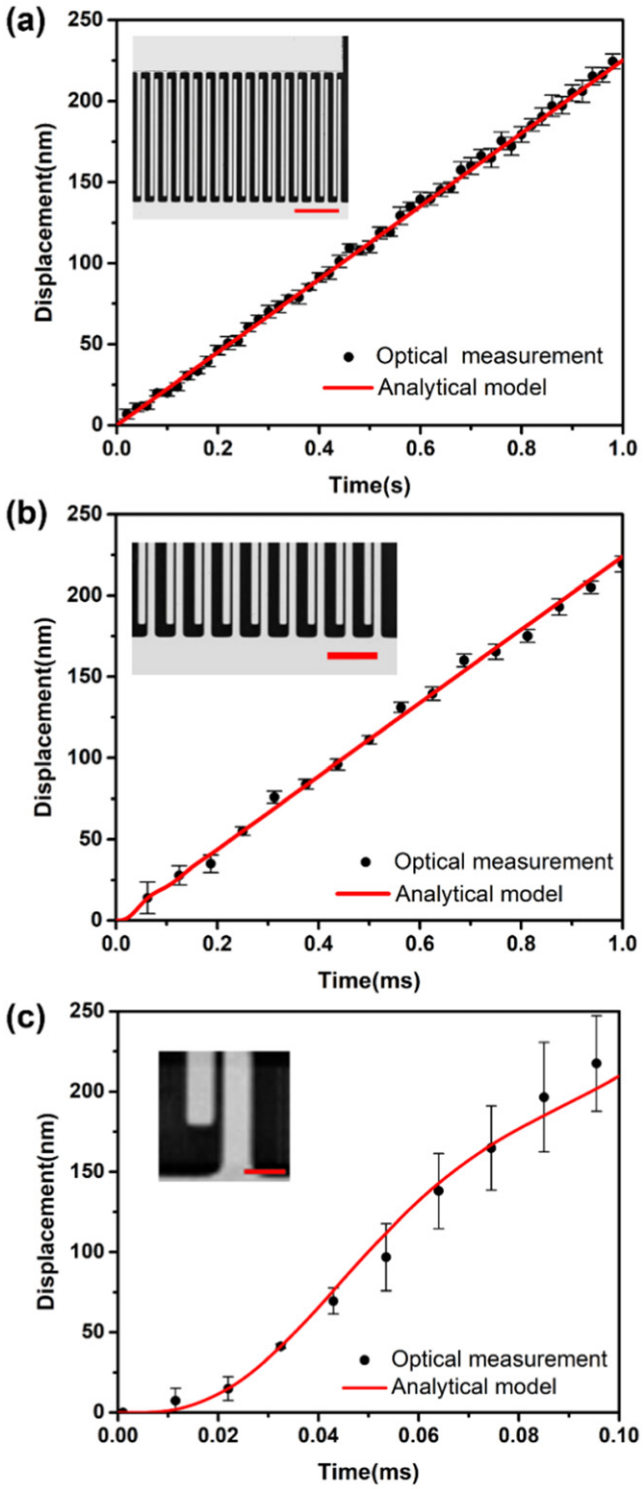


**Fig. 8** Comparison of displacements from the dynamics model and measured optically in air when loading time is (a) 1 s, (b) 1 ms, and (c) 0.1 ms. The frame rates are 50, 16,000, and 95,000 fps, respectively. Insets are the corresponding images. Scale bars are 100, 50, and 10 μm, respectively. A higher frame rate is associated with a smaller field of view. Reproduced from Li, C., Zhang, D., Cheng, G., Zhu, Y., 2020b. Microelectromechanical systems for nanomechanical testing: Electrostatic actuation and capacitive sensing for high-strain-rate testing. Exp. Mech. 60, 329–343. https://doi.org/10.1007/S11340-019-00565-5/FIGURES/15.

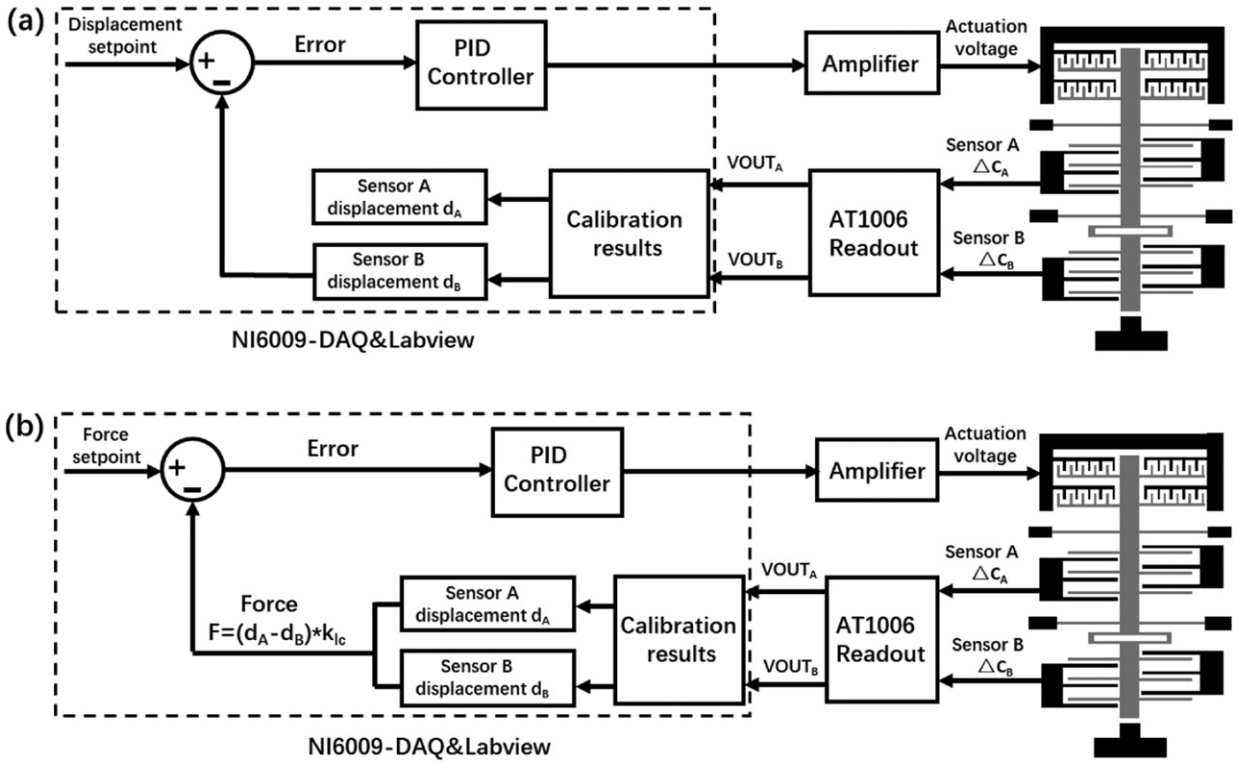


**Fig. 9** Closed-loop block diagrams for (a) displacement control and (b) force control. Reproduced from Li, C., Cheng, G., Wang, H., Zhu, Y., 2020a. Microelectromechanical systems for nanomechanical testing: Displacement- and force-controlled tensile testing with feedback control. Exp. Mech. 60, 1005–1015. https://doi.org/10.1007/s11340-020-00619-z.

proportional–integral–derivative (PID) controller directly on the electrostatic actuator. Both elongation and force of the specimen can be obtained electronically in real time. (**Fig. 9**).

Three representative tests – stress relaxation and creep of penta-twinned Ag NWs, and tensile test of single-crystalline Au NWs with sudden stress drop – were carried out to demonstrate the displacement- and force-controlled tensile testing of nanostructures. The activation volumes were extracted from the stress relaxation and creep tests, which indicated that additional dislocation mechanisms (e.g., dislocation-twin boundary interactions) exist in addition to surface dislocation nucleation in penta-twinned Ag NWs.

Take the stress relaxation tests of the penta-twinned Ag NWs as an example. It was previously found that penta-twinned Ag NWs exhibit stress relaxation as a result of vacancy diffusion assisted dislocation nucleation (Qin *et al.*, 2015). However, the MEMS platform used was not capable of displacement control. An otherwise identical experiment except under displacement control was conducted with the newly developed MEMS platform, where a true stress relaxation test was realized. **Fig. 10**(a) shows the stress-strain curve of the specimen tested, with the corresponding strain versus time and stress versus time relationships shown in **Fig. 10**(b) and (c), respectively. It can be seen that the stress relaxed during the holding period while the strain remained constant. **Fig. 10**(d) shows the change in the resolved shear stress as a function of time. The apparent activation volume, $5.70b^3$, was obtained by fitting the stress relaxation data (**Fig. 10**(d)), where $b$ denotes the magnitude of the Burgers vector.

## Fatigue Testing

In-situ TEM fatigue tests with the MEMS platforms can provide unprecedented details about the local microstructural processes that govern damage accumulation, crack nucleation, and crack propagation during the fatigue loading. For fatigue testing, it is necessary to conduct force and displacement measurements electronically, as the imaging is likely not fast enough. The P2P device from Hysitron has been used to study fatigue (Bufford *et al.*, 2016). Pierron and co-workers have developed a dedicated MEMS platform that consists of two separated capacitive sensors that can measure the force and displacement simultaneously and independently (Hosseinian and Pierron, 2013; Pant *et al.*, 2011). This platform can also be used for ex-situ experiments that could investigate environmental effect in air.

Fatigue behavior typically includes three types: (1) cyclic plasticity and ratcheting above the yield strength, (2) low-cycle fatigue in the vicinity of the yield strength with fatigue life $\sim 10$–$10^3$ cycles, and (3) high-cycle fatigue well below the yield strength with fatigue life over $10^4$ cycles. Espinosa and co-workers reported cyclic tensile testing of penta-twinned Ag NWs above the yield strength, using their MEMS tensile testing platform (Bernal *et al.*, 2015). Upon unloading, Bauschinger effect,

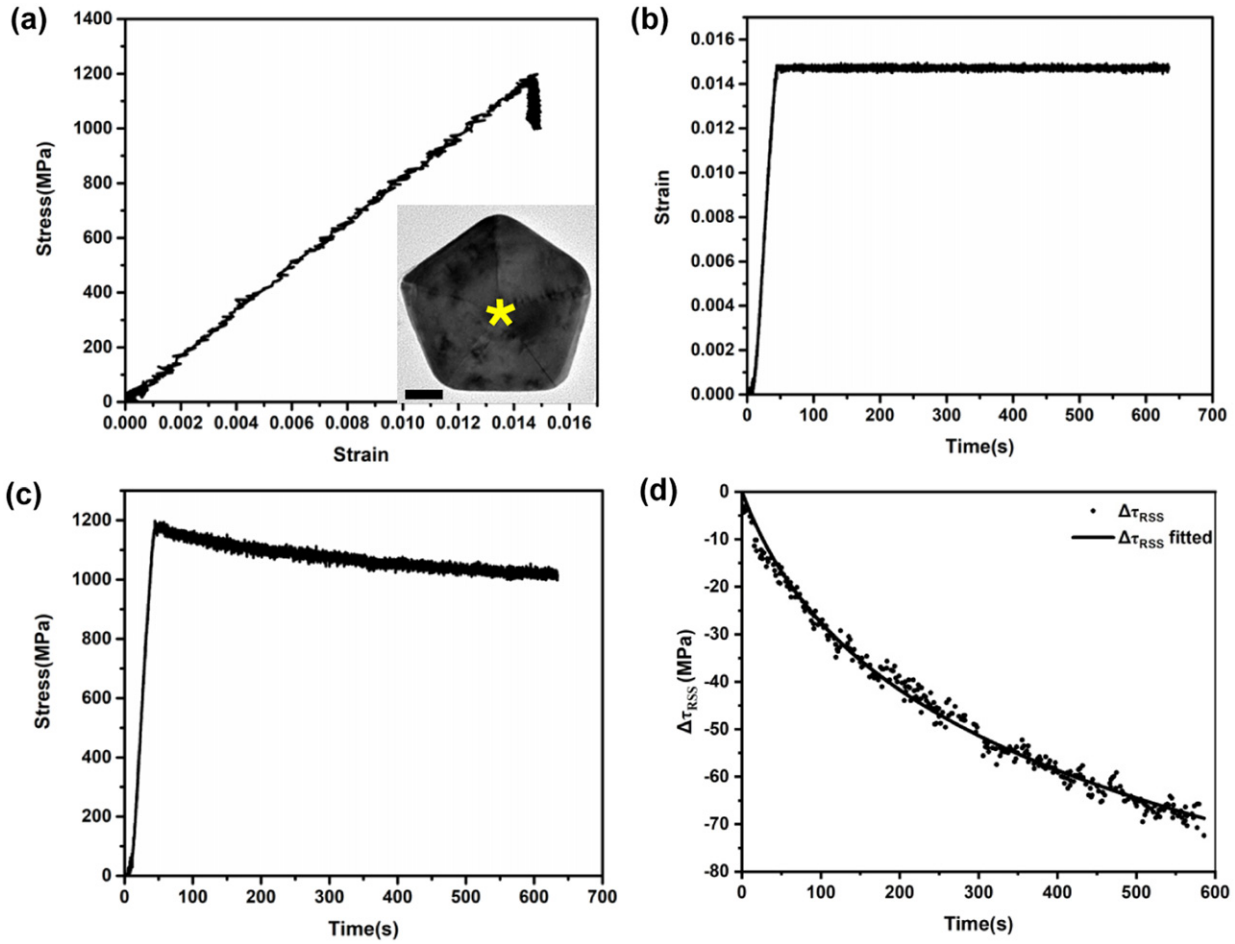


**Fig. 10** Stress relaxation of a penta-twinned Ag NW. (a) Stress vs. strain. Insert is the cross-sectional TEM image of the tested NW, scale bar, 20 nm. (b) Strain vs. time. (c) Stress vs. time. (d) Experimental data and fitted curve of the shear stress decrease vs. time. Reproduced from Li, C., Cheng, G., Wang, H., Zhu, Y., 2020a. Microelectromechanical systems for nanomechanical testing: Displacement- and force-controlled tensile testing with feedback control. Exp. Mech. 60, 1005–1015. https://doi.org/10.1007/s11340-020-00619-z.

asymmetric plastic flow, and partial recovery of the plastic deformation were observed (**Fig. 11**(a)). In-situ TEM and atomistic simulations found that these processes are attributed to the reversible dislocation activity. It has been previously found that the dislocation mechanism in penta-twinned NWs is the stacking fault decahedrons (SFDs). The incipient plastic mechanism through the nucleation of SFDs is fully reversible, but plasticity becomes only partially reversible as intersecting SFDs lead to dislocation reactions and entanglements. The same phenomenon was observed independently by Zhu and co-workers (Qin *et al.*, 2015).

Using the "two-sensor" platform, Hosseinian and Pierron have investigated the fatigue of Au nanobeams with the grain size ranging from 10 to 400 nm (Hosseinian and Pierron, 2013). Fatigue tests were carried out both ex-situ and by in-situ TEM. In the ex-situ test, the specimen failed after 11,125 cycles and a ratcheting behavior was observed. But no obvious change in the microstructure was observed from post-mortem TEM images. Next an in-situ TEM fatigue testing was preformed to observe the microstructure evolution. The specimen failed at 6995 cycles with the same ratcheting behavior (**Fig. 11**(b)). During the in-situ TEM test, a large number of dislocations were found to nucleate after 400 cycles, accompanied with twins and stacking faults. After fracture a large number of dislocations can be seen near the fracture plane.

Using the P2P platform, Bufford *et al.* (2016) investigated high cycle fatigue of nanocrystalline Cu films by in-situ TEM. Controllable loads were applied at frequencies from one to several hundred Hz, enabling accumulations of $10^6$ cycles per hour. In-situ TEM allowed measurement of slow crack extension rates, $\sim 10^{-12}$ m $\cdot$ cycle$^{-1}$, with a load well below the tensile yield strength. Evidence of localized deformation and grain growth within 150 nm of the crack tip was observed by both standard TEM imaging and diffraction-based orientation mapping (**Fig. 11**(c)). Enlarged grains with different orientations were found in the immediate vicinity of the crack initiation site and stable propagation path. Areas of interest were readily tracked by TEM in real time. For analytical techniques requiring longer data acquisition times, loading experiments were periodically paused and then resumed later.

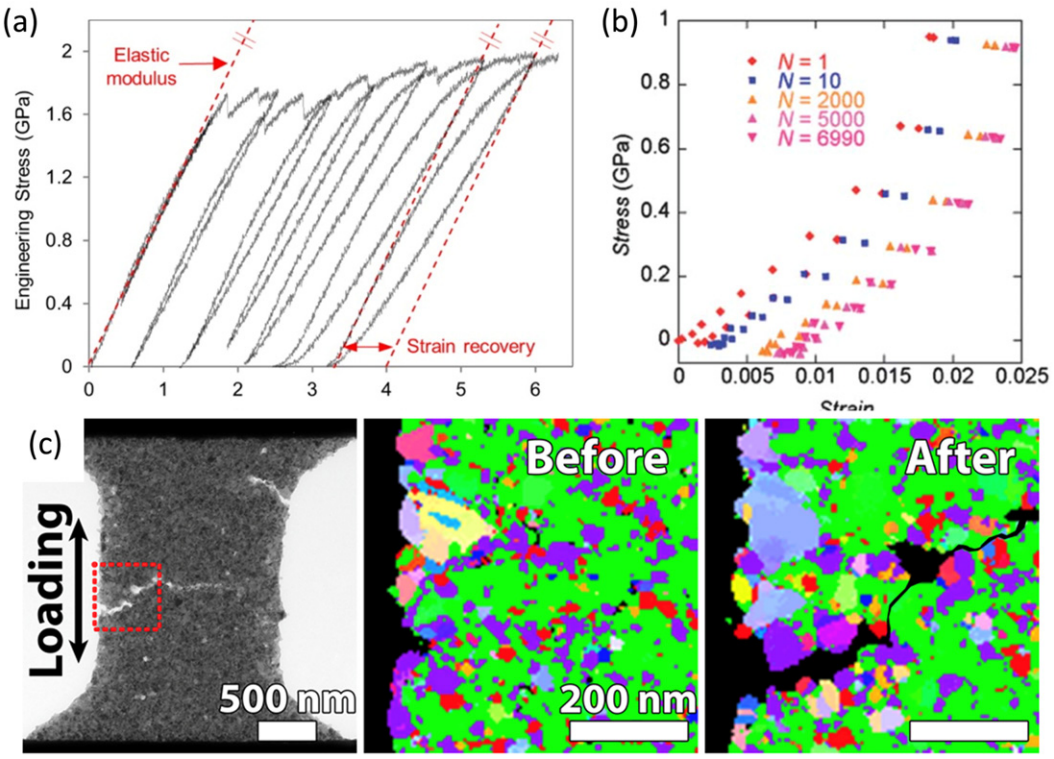


**Fig. 11** MEMS-based in-situ TEM fatigue tests. (a) Cyclic plasticity in Ag NWs. (b) Low cycle fatigue of Ag nanobeams. (c) High cycle fatigue of Cu films. Crystallographic orientation maps of the same area (boxed area in the left panel) collected before loading and after sample failure are shown with the crack path traced. Reproduced from Bernal, R.A., Aghaei, A., Lee, S., *et al.*, 2015. Intrinsic Bauschinger effect and recoverable plasticity in pentatwinned silver nanowires tested in tension. Nano Lett. 15, 139–146. https://doi.org/10.1021/nl503237t. Hosseinian, E., Pierron, O.N. 2013. Quantitative in situ TEM tensile fatigue testing on nanocrystalline metallic ultrathin films. Nanoscale 5: 12532–12541. https://doi.org/10.1039/c3nr04035f. Bufford, D.C., Stauffer, D., Mook, W.M., *et al.*, 2016. High cycle fatigue in the transmission electron microscope. Nano Lett. 16, 4946–4953. https://doi.org/10.1021/ACS.NANOLETT.6B01560/SUPPL_FILE/NL6B01560_SI_001.PDF.

## Thermomechanical Testing

For device applications it is inevitable for nanostructures to experience different temperatures. Thus, it is of relevance to characterize their thermomechanical behavior. Kang and Saif developed a MEMS platform for in-situ uniaxial test of micro/nanoscale samples at high temperature (Kang and Saif, 2011). Fabricated out of SiC, this platform was able to sustain temperature up to 700°C, which is much higher than those made of Si. Based on their earlier design (Haque and Saif, 2002a), Joule heating was incorporated for heating while a local bi-metal type temperature sensor was used for temperature measurement. The platform was extended for bending tests under elevated temperature, which was used to study the possible size effect on the BDT temperature of Si. Their results. showed that the BDT temperature of Si reduces with sample size, e.g., 293°C for a sample size of 720 nm (Kang and Saif, 2013). Microfabricated heaters have also been integrated to a thermomechanical testing platform for testing microscale films (Sim *et al.*, 2013).

Chen *et al.* integrated their MEMS platform inside a vacuum cryostat including a heater, a cooling channel with liquid nitrogen circulation and a PID temperature controller (Chen *et al.*, 2014). The vacuum chamber has a fused silica window on top so that the MEMS platform inside can be viewed by an optical microscope. Their setup is capable of achieving temperature range from 77 to 475K. The authors tested $< 110 >$ Pd NWs using the setup and found the NW strength varies as a function of temperature (Chen *et al.*, 2015). In particular, they found a clear decline in yield strength with increasing temperature, which implies that surface dislocation nucleation is assisted by thermal fluctuations. It is well known now that for nanostructures with diameter less than ~100 nm (e.g., NWs), the dominant dislocation mechanism is surface dislocation nucleation. However, the origin of the surface dislocation nucleation remains elusive. In this work the authors speculated that surface diffusion might play an important role in the initiating the surface dislocation nucleation.

Chang and Zhu (2013) has developed a MEMS thermomechanical platform with an on-chip heater for in-situ mechanical testing of 1D nanostructures from room temperature to 600K. The MEMS platform consists of a comb-drive actuator, a capacitive load sensor, a specimen gap, and a heater based on Joule heating in close proximity to the specimen gap, as shown in **Fig. 12**. The entire platform is symmetric to ensure the same temperature on both sides of the specimen to avoid temperature gradient and heat flow through the specimen. The temperature distribution in air was measured by Raman spectroscopy. Fully 3D multiphysics simulation was used to predict the temperature distribution in vacuum. The heater consists of multiple Z-shaped beams, whose dimensions were carefully designed in order to purposely compensate the thermal expansion of the long axial shuttles of the actuator and sensor.

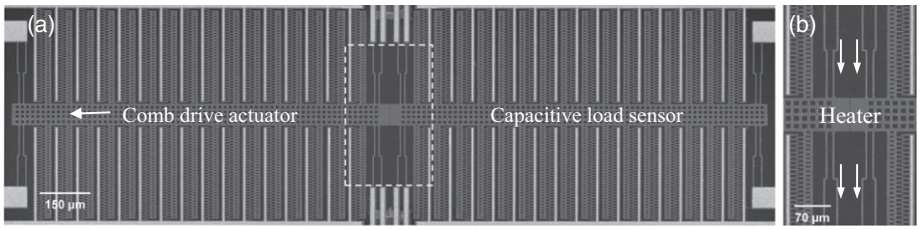


**Fig. 12** (a) SEM image of the thermomechanical MEMS platform that consists of three parts: comb drive actuator, capacitive load sensor, and heater. (b) Magnified view of the heater as boxed in (a). The arrows indicate the current direction. Reproduced from Chang, T.-H., Zhu, Y., 2013. A microelectromechanical system for thermomechanical testing of nanostructures. Appl. Phys. Lett. 103, 263114. https://doi.org/10.1063/1.4858962.

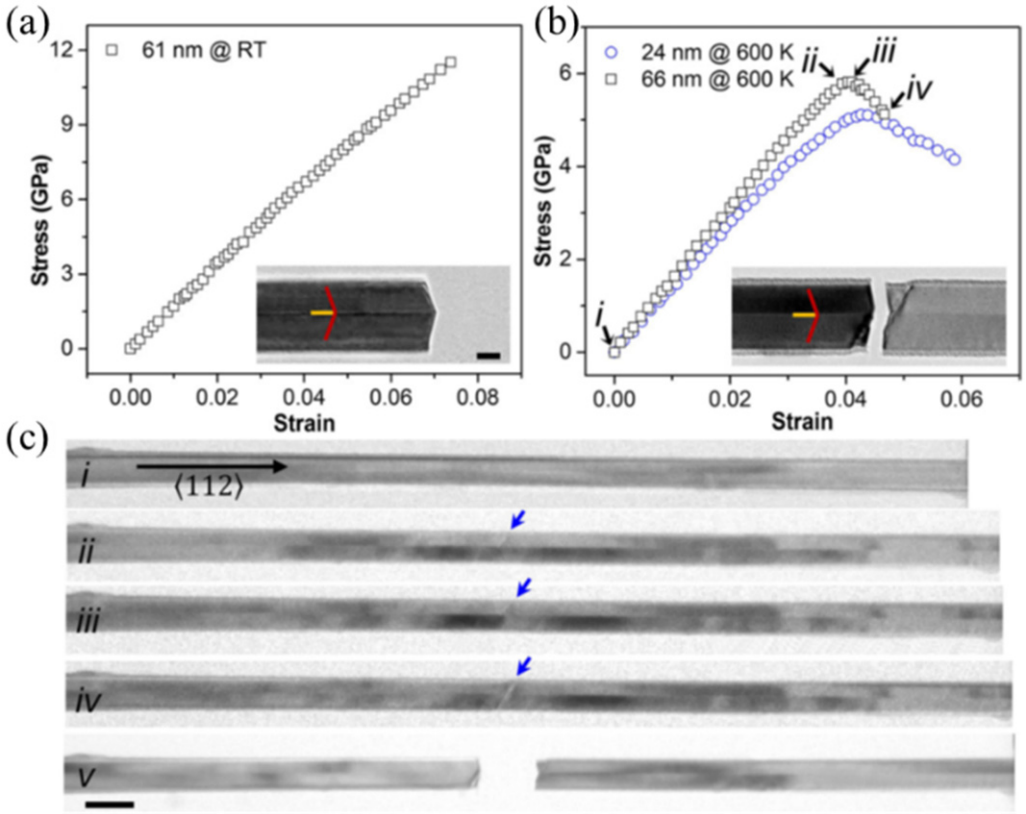


**Fig. 13** In situ MEMS-based measurement and TEM observation of mechanical behavior of individual Si NWs under uniaxial tension at room and elevated temperatures. (a,b) Stress–strain curves of Si NWs tested at 295 and 600K, respectively. Insets in (a,b) are the corresponding fracture morphologies of the tested NWs with diameters of 61 and 66 nm, respectively. Scale bar, 20 nm. (c) Snapshots of microstructure evolution corresponding to (b). Reproduced from Cheng, G., Zhang, Y., Chang, T.-H., *et al.*, 2019. In Situ nano-thermomechanical experiment reveals brittle to ductile transition in silicon nanowires. Nano Lett. 19, 5327–5334. Available at: https://doi.org/10.1021/acs.nanolett.9b01789.

Brittle to ductile transition (BDT) has been extensively studied for bulk Si. However, it remains unclear how BDT in Si NWs is affected by the NW size and in particular if Si NWs become ductile at room temperature. Several studies showed that Si NWs behave linear elastically until brittle fracture under tension (Gordon *et al.*, 2009; Tang *et al.*, 2012; Zhang *et al.*, 2016; Zhu *et al.*, 2009); by contrast, other studies demonstrated that Si NWs could exhibit substantial plastic deformation under tension (Han *et al.*, 2007) and especially under bending (Elhebeary *et al.*, 2020; Kang and Saif, 2013; Tang *et al.*, 2012). Using the in-situ thermomechanical testing device discussed above, Cheng *et al.* found that Si NWs are brittle at room temperature but exhibits ductile behavior with dislocation-mediated plasticity at elevated temperature by in-situ temperature-controlled nanomechanical tensile testing in TEM (Cheng *et al.*, 2019). Si NWs were synthesized by chemical vapor deposition (CVD) following a vapor-liquid-solid (VLS) process (Wu *et al.*, 2004; Zhu *et al.*, 2009), with $< 112 >$ axial orientation and a single TB along the NW length. 78 Si NWs were tested between room temperature and 600K, with representative results shown in **Fig. 13**. The testing results revealed that unconventional $\frac{1}{2}< 110 > \{001\}$ dislocations become highly active with increasing temperature, resulting in the transition from brittle fracture to dislocation-mediated plasticity and ductile fracture at elevated temperature.

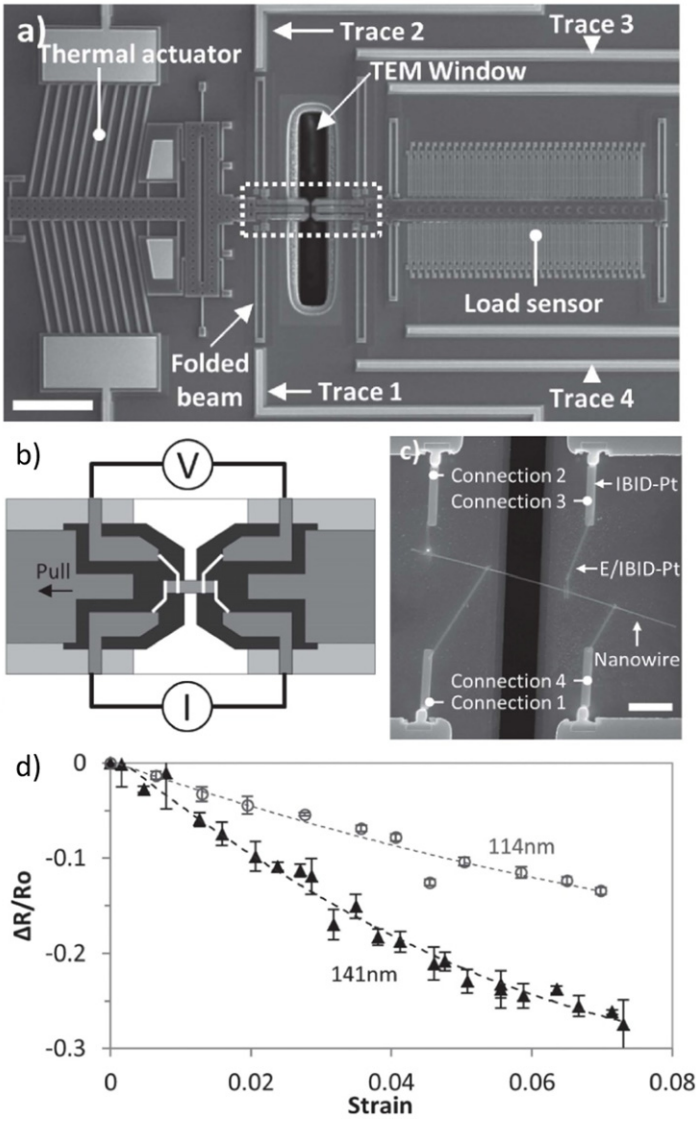


**Fig. 14** (a) Overview of the MEMS platform. (b) Schematic and (c) SEM image of a NW laid on an insulating shuttle and connected in the four-point configuration. (d) Relative resistance change of two Si NW samples as a function of strain. Reproduced from Bernal, R.A., Filleter, T., Connell, J., *et al.*, 2014. In situ electron microscopy four-point electromechanical characterization of freestanding metallic and semiconducting nanowires. Small 10, 725–733. https://doi.org/10.1002/smll.201300736.

## Electromechanical Testing

It is of fundamental and technological importance to understand the multiphysical coupling in nanostructures. Of particular interest is the co-called elastic strain engineering, that is, how mechanical strain can affect other physical and chemical properties such as electronic, optical, magnetic, phononic, and catalytic properties. Nanostructures typically exhibit ultrahigh mechanical strength, thus offering unprecedentedly large room for elastic strain engineering. Bernal *et al.* has developed a MEMS platform to characterize electromechanical coupling of NWs using the MUMPs-PLUS process (MEMSCAP, Durham, NC) that includes a silicon nitride layer beneath the polysilicon structural layer for electric isolation (Bernal *et al.*, 2014). Based on the original design that consists of a thermal actuator, a specimen gap and a load sensor (Zhu *et al.*, 2006), four conductive support beams plus four deposited Pt lines form the four electrical paths for the four-point measurement, as shown in **Fig. 14**(a), (b), and (c). Penta-twinned Ag NWs and Si NWs were tested representative of metallic and semiconductor NWs, respectively. For the Ag NWs, the resistance variations were attributed to the NW dimensional changes; while for the Si NWs, the piezoresistance coefficients were found to be similar to bulk values (**Fig. 14**(d)).

Zhang *et al.* (2011) fabricated an electromechanical MEMS platform based on a standard SOI process, but with a $SiO_2$ layer beneath the structural layer for electrical isolation. The authors investigated piezoresistivity of Si NWs using the platform and found that e-beam irradiation during SEM imaging can have a significant effect on the I–V characteristics of the NWs. Kiuchi *et al.* (2008) fabricated an electromechanical MEMS platform based on their previous mechanical platform (Kiuchi *et al.*, 2007).

Electrical resistance of carbon NWs was measured as a function of strain. The gauge factor was measured to be 0.7 below a tensile strain of 4% but −0.9 above 4%. Note that an external Kelvin bridge method was used for the resistance measurement.

Murphy *et al.* (2014) studied thermal conductivity of Si NWs as a function of tensile strain. A MEMS platform was used to apply tensile strain to the specimen, while Raman spectroscopy was used to measure its thermal conductivity. Their results showed that phononic transport in undoped Si NWs (diameter range 170–180 nm) is largely unaffected by uniform tensile strain, but point defects introduced via ion bombardment can reduce the thermal conductivity by over 70%.

Using photoluminescence and Raman spectroscopy, optomechanical behavior of direct-bandgap NWs (e.g., Ge and GaAs NWs) was investigated (Greil *et al.*, 2012; Signorello *et al.*, 2014, 2013). Compared to bulk Ge, an anomalously high and negative-signed piezoresistive coefficient was found (Greil *et al.*, 2012). A rapid decrease in resistivity and a red-shift in photocurrent spectra was reported for GaAs NWs under high tensile strain (Signorello *et al.*, 2013). A small uniaxial stress was found to induce a reversible direct-to-pseudodirect band structure transition, which can switch on and off luminescence of wurtzite GaAs NWs (Signorello *et al.*, 2014). Of note is that most MEMS-based in-situ testing has been performed inside SEM or TEM. Integration of MEMS platforms with other types of microscopy or spectroscopy could offer exciting opportunities for mechanical testing especially multiphysical testing of nanostructures.

## Summary and Outlook

We have reviewed the recent advances in the field of mechanical characterization of 1D nanostructures using MEMS platforms. Many different types of MEMS platforms have been designed, fabricated and employed for nanomechanical testing including basic tensile testing, high-strain-rate testing, creep and stress relaxation, fatigue testing, thermomechanical testing, and multiphysical testing. A large number of nanostructures have been characterized including carbon nanotubes, metallic NWs, semiconductor NWs, ceramic NWs, and polymer nanofibers. MEMS platforms have significantly facilitated to our studies of the nanoscale mechanical behaviors.

It is worth noting that much of the early nanomechanical measurements revealed significant scatter and discrepancy, which is understandable considering the infancy of the field, the challenge of conducting such measurements, and the differences in the shape and microstructures of the specimens. With continued advance in testing methods and careful consideration of the factors mentioned above, more consistent testing results have been and will continue to emerge. For example, efforts have been taken on systematic examination of the effects of sample cross sections (Chang *et al.*, 2016) and microstructures (Bernal *et al.*, 2015; Qin *et al.*, 2015; Wang *et al.*, 2013), loading modes (Chang *et al.*, 2016; Xu *et al.*, 2010), and boundary conditions (Murphy *et al.*, 2013; Qin *et al.*, 2012).

In addition to the basic mechanical properties (e.g., Young's modulus, yield strength, and fracture strength), advanced behaviors and deformation processes of nanostructures have gained increasing interest. Such behaviors are dependent on the temperature, strain rate, time, and environment, among other variables, which are of direct relevance to service life of nanostructures. Multiphysical properties of nanostructures are of particular interest. Given the large elastic strain range of NWs, they are ideal candidates to tune other properties (e.g., electric, thermal, optical, catalytic) using elastic strain.

With the recent advance in electron microscopy (Campbell *et al.*, 2014) (e.g., dynamic transmission electron microscopy, DTEM (Kim *et al.*, 2008) and 4D scanning transmission electron microscopy, 4D-STEM (Ophus, 2019)), it might become possible to capture the dynamic response of nanostructures with atomic resolution. Combination of MEMS and advanced electron microscopy, together with the limited volume of nanostructures, could offer exciting opportunities for probing the nanoscale mechanical and other physical behaviors. Beyond electron microscopy, it is promising to combine MEMS platforms with atomic force microscopy (Chasiotis and Knauss, 2002; Elhebeary *et al.*, 2020) and spectroscopic methods such as Raman spectroscopy (Spolenak *et al.*, 2010) and photoluminescence spectroscopy (Sun *et al.*, 2013).

As the number of atoms in the nanostructures comes increasingly within the reach of the state-of-the-art computational modeling capabilities, comparison between nanomechanical tests and MD simulations has become closer to reality. However, the well-known challenge is that MD simulations operate at time scales (hundreds of nanoseconds) and strain rates ($10^6\ s^{-1}$ and above) that are orders of magnitude faster than seen experimentally. While recent efforts in both experiments (Li *et al.*, 2020b; Ramachandramoorthy *et al.*, 2016) and simulations (Tao *et al.*, 2018; Yan *et al.*, 2016; Yan and Sharma, 2016; Zhu *et al.*, 2008) have been made to bridge the gap, further work is warranted to realize true comparison between nanomechanical tests and MD simulations side by side, which holds great promise to elucidate the nanoscale deformation behaviors.

2D materials including graphene, hexagonal boron nitride, transition metal dichalcogenide, and MXenes have received extensive interests (Akinwande *et al.*, 2017; Dai *et al.*, 2019). Their mechanical properties including interfacial properties have been investigated mostly on a stretchable substrate (Cao *et al.*, 2014; Jiang *et al.*, 2014; Jiang and Zhu, 2015; Na *et al.*, 2016; Papageorgiou *et al.*, 2017). MEMS platforms have been recently used to study mechanical properties of freestanding 2D materials (Cao *et al.*, 2020; Yang *et al.*, 2021; Zhang *et al.*, 2014). This is a relatively new and open field. MEMS platforms with all the advanced testing capabilities such as temperature, strain rate, and displacement control could be very valuable for mechanical testing of 2D materials.

## Acknowledgment

We would like to gratefully acknowledge the financial support of the National Science Foundation (NSF) under Award Nos. 1762511 and 1929646.

## References


Abbas, K., Alaie, S., Leseman, Z.C., 2012. Design and characterization of a low temperature gradient and large displacement thermal actuators for in situ mechanical testing of nanoscale materials. J. Micromech. Microeng. 22. 125027. https://doi.org/10.1088/0960-1317/22/12/125027.

Agrawal, R., Peng, B., Espinosa, H.D., 2009. Experimental-computational investigation of ZnO nanowires strength and fracture. Nano Lett. 9, 4177–4183.

Agrawal, R., Loh, O., Espinosa, H.D., 2011. The evolving role of experimental mechanics in 1-D nanostructure-based device development. Exp. Mech. 51, 1–9.

Agrawal, R., Peng, B., Gdoutos, E.E., Espinosa, H.D., 2008. Elasticity size effects in ZnO nanowires–a combined experimental-computational approach. Nano Lett. 8, 3668–3674. https://doi.org/10.1021/nl801724b.

Akinwande, D., Brennan, C.J., Bunch, J.S., *et al.*, 2017. A review on mechanics and mechanical properties of 2D materials – Graphene and beyond. Extreme Mech. Lett. 13, 42–77. https://doi.org/10.1016/J.EML.2017.01.008.

Barlian, A.A., Park, W.-T., Mallon, J.R., Rastegar, A.J., Pruitt, B.L., 2009. Review: Semiconductor piezoresistance for microsystems. Proc. IEEE. Inst. Electr. Electron. Eng. 97, 513–552. https://doi.org/10.1109/JPROC.2009.2013612.

Bernal, R.A., Agrawal, R., Peng, B., *et al.*, 2011. Effect of growth orientation and diameter on the elasticity of gan nanowires. A combined in Situ TEM and atomistic modeling investigation. Nano Lett. 11, 548–555. https://doi.org/10.1021/nl103450e.

Bernal, R.A., Filleter, T., Connell, J., *et al.*, 2014. In situ electron microscopy four-point electromechanical characterization of freestanding metallic and semiconducting nanowires. Small 10, 725–733. https://doi.org/10.1002/smll.201300736.

Bernal, R.A., Aghaei, A., Lee, S., *et al.*, 2015. Intrinsic Bauschinger effect and recoverable plasticity in pentatwinned silver nanowires tested in tension. Nano Lett. 15, 139–146. https://doi.org/10.1021/nl503237t.

Boser, B.E., Howe, R.T., 1996. Surface micromachined accelerometers. IEEE J. Solid-State Circuits 31, 366–375.

Brown, J.J., Baca, A.I., Bertness, K.a, *et al.*, 2011. Tensile measurement of single crystal gallium nitride nanowires on MEMS test stages. Sens. Actuators A Phys. 166, 177–186. https://doi.org/10.1016/j.sna.2010.04.002.

Brown, J.J., Suk, J.W., Singh, G., *et al.*, 2009. Microsystem for nanofiber electromechanical measurements. Sens. Actuators A Phys. 155, 1–7. https://doi.org/10.1016/j.sna.2008.11.001.

Bufford, D.C., Stauffer, D., Mook, W.M., *et al.*, 2016. High cycle fatigue in the transmission electron microscope. Nano Lett. 16, 4946–4953. https://doi.org/10.1021/ACS.NANOLETT.6B01560/SUPPL_FILE/NL6B01560_SI_001.PDF.

Campbell, G.H., McKeown, J.T., Santala, M.K., 2014. Time resolved electron microscopy for in situ experiments. Appl. Phys. Rev. 1.https://doi.org/10.1063/1.4900509. 041101.

Cao, K., Feng, S., Han, Y., *et al.*, 2020. Elastic straining of free-standing monolayer graphene. Nat. Commun. 111 (11), 1–7. https://doi.org/10.1038/s41467-019-14130-0.

Cao, Z., Wang, P., Gao, W., *et al.*, 2014. A blister test for interfacial adhesion of large-scale transferred graphene. Carbon 69, 390–400. https://doi.org/10.1016/J.CARBON.2013.12.041.

Chan, C.K., Peng, H.L., Liu, G., *et al.*, 2008. High-performance lithium battery anodes using silicon nanowires. Nat. Nanotechnol. 3, 31–35.

Chang, T.-H., Zhu, Y., 2013. A microelectromechanical system for thermomechanical testing of nanostructures. Appl. Phys. Lett. 103. 263114. https://doi.org/10.1063/1.4858962.

Chang, T.-H., Cheng, G., Li, C., Zhu, Y., 2016. On the size-dependent elasticity of penta-twinned silver nanowires. Extreme Mech. Lett. 8, 177–183. https://doi.org/10.1016/j.eml.2016.03.007.

Chasiotis, I., Knauss, W.G., 2002. A new microtensile tester for the study of MEMS materials with the aid of atomic force microscopy. Exp. Mech. 42, 51–57.

Chen, C.Q., Shi, Y., Zhang, Y.S., Zhu, J., Yan, Y.J., 2006. Size dependence of the Young's modulus of ZnO nanowires. Phys. Rev. Lett. 96. 75505.

Chen, L., Richter, G., Sullivan, J., Gianola, D., 2012. Lattice anharmonicity in defect-free Pd nanowhiskers. Phys. Rev. Lett. 109. 125503. https://doi.org/10.1103/PhysRevLett.109.125503.

Chen, L.Y., He, M.-R., Shin, J., Richter, G., Gianola, D.S., 2015. Measuring surface dislocation nucleation in defect-scarce nanostructures. Nat. Mater. 14, 707–713. https://doi.org/10.1038/nmat4288.

Chen, L.Y., Terrab, S., Murphy, K.F., *et al.*, 2014. Temperature controlled tensile testing of individual nanowires. Rev. Sci. Instrum. 85. 013901. https://doi.org/10.1063/1.4858815.

Cheng, G., Chang, T.-H., Qin, Q., Huang, H., Zhu, Y., 2014. Mechanical properties of silicon carbide nanowires: effect of size-dependent defect density. Nano Lett. 14, 754–758. https://doi.org/10.1021/nl404058r.

Cheng, G., Yin, S., Chang, T.-H., *et al.*, 2017. Anomalous tensile detwinning in twinned nanowires. Phys. Rev. Lett. 119. 256101. https://doi.org/10.1103/PhysRevLett.119.256101.

Cheng, G., Yin, S., Li, C., *et al.*, 2020. In-situ TEM study of dislocation interaction with twin boundary and retraction in twinned metallic nanowires. Acta Mater. 196, 304–312. https://doi.org/10.1016/j.actamat.2020.06.055.

Cheng, G., Zhang, Y., Chang, T.-H., *et al.*, 2019. In Situ nano-thermomechanical experiment reveals brittle to ductile transition in silicon nanowires. Nano Lett. 19, 5327–5334. https://doi.org/10.1021/acs.nanolett.9b01789.

Chisholm, C., Bei, H., Lowry, M.B., *et al.*, 2012. Dislocation starvation and exhaustion hardening in Mo alloy nanofibers. Acta Mater. 60, 2258–2264. https://doi.org/10.1016/j.actamat.2011.12.027.

Dai, Z., Liu, L., Zhang, Z., *et al.*, 2019. Strain engineering of 2D materials: Issues and opportunities at the interface. Adv. Mater. 31.https://doi.org/10.1002/ADMA.201805417. 1805417.

Desai, A.V., Haque, M.A., 2007. Mechanical properties of ZnO nanowires. Sens. Actuators Phys. 134, 169–176.

Diao, J., Gall, K., Dunn, M.L., 2003. Surface-stress-induced phase transformation in metal nanowires. Nat. Mater. 2, 656–660.

Durelli, A.J., Morse, S., Parks, V., 1962. Theta specimen for determining tensile strength of brittle materials. Mater. Res. 2, 114–117.

Elhebeary, M., Harzer, T., Dehm, G., Saif, M.T.A., 2020. Time-dependent plasticity in silicon microbeams mediated by dislocation nucleation. Proc. Natl. Acad. Sci. USA 117, 16864–16871. https://doi.org/10.1073/PNAS.2002681117.

Espinosa, H.D., Zhu, Y., Moldovan, N., 2007. Design and operation of a MEMS-based material testing system for nanomechanical characterization. J. Microelectromech. Syst. 16, 1219–1231.

Espinosa, H.D., Bernal, R.A., Filleter, T., 2012. In situ TEM electromechanical testing of nanowires and nanotubes. Small 8, 3233–3252. https://doi.org/10.1002/smll.201200342.

Fan, Z.Y., Ho, J.C., Takahashi, T., *et al.*, 2009. Toward the development of printable nanowire electronics and sensors. Adv. Mater. 21, 3730–3743.

Feng, X.L., He, R., Yang, P., Roukes, M.L., 2007. Very high frequency silicon nanowire electromechanical resonators. Nano Lett. 7, 1953–1959.

Filleter, T., Ryu, S., Kang, K., *et al.*, 2012. Nucleation-controlled distributed plasticity in penta-twinned silver nanowires. Small 8, 2986–2993. https://doi.org/10.1002/smll.201200522.

Gaither, M.S., DelRio, F.W., Gates, R.S., Cook, R.F., 2011. Deformation and fracture of single-crystal silicon theta-like specimens. J. Mater. Res. 26, 2575–2589.

Ganesan, Y., Peng, C., Lu, Y., *et al.*, 2010. Effect of nitrogen doping on the mechanical properties of carbon nanotubes. ACS Nano 4, 7637–7643.

Gianola, D.S., Eberl, C., 2009. Micro-and nanoscale tensile testing of materials. JOM 61, 24.

Gordon, M.J., Baron, T., Dhalluin, F., Gentile, P., Ferret, P., 2009. Size effects in mechanical deformation and fracture of cantilevered silicon nanowires. Nano Lett. 9, 525–529.

Greil, J., Lugstein, A, Zeiner, C., Strasser, G., Bertagnolli, E., 2012. Tuning the electro-optical properties of germanium nanowires by tensile strain. Nano Lett. 12, 6230–6234. https://doi.org/10.1021/nl303288g.

Guan, C., Zhu, Y., 2010a. An electrothermal microactuator with Z-shaped beams. J. Micromech. Microeng. 20.https://doi.org/10.1088/0960-1317/20/8/085014. 085014.

Guan, C.H., Zhu, Y., 2010b. Z-shaped electrothermal microactuators: Design and operation. J. Micromech. Microeng. 20. 85014.

Guo, H., Wang, K., Deng, Y., *et al.*, 2013. Nanomechanical actuation from phase transitions in individual VO2 micro-beams. Appl. Phys. Lett. 102. 231909. https://doi.org/10.1063/1.4810872.

Guo, H., Chen, K., Oh, Y., *et al.*, 2011. Mechanics and dynamics of the strain-induced M1-M2 structural phase transition in individual VO2 nanowires. Nano Lett. 11, 3207–3213. https://doi.org/10.1021/nl201460v.

Han, J.H., Saif, M.T.A., 2006. In situ microtensile stage for electromechanical characterization of nanoscale freestanding films. Rev. Sci. Instrum. 77. 045102. https://doi.org/10.1063/1.2188368.
Han, X., Zheng, K., Zhang, Y.F., *et al.*, 2007. Low-temperature in situ large-strain plasticity of silicon nanowires. Adv. Mater. 19, 2112–2118.
Haque, M.A., Saif, M.T.A., 2002a. In-situ tensile testing of nano-scale specimens in SEM and TEM. Exp. Mech. 42, 123–128.
Haque, M.A., Saif, M.T.A., 2002b. Application of MEMS force sensors for in situ mechanical characterization of nano-scale thin films in SEM and TEM. Sens. Actuators A Phys. 97–8, 239–245.
Haque, M.A., Saif, M.T.A., 2004. Deformation mechanisms in free-standing nanoscale thin films: A quantitative in situ transmission electron microscope study. Proc. Natl. Acad. Sci. USA 101, 6335–6340.
Haque, M.A., Espinosa, H.D., Lee, H.J., 2011. MEMS for In situ testing—handling, actuation, loading, and displacement measurements. MRS Bull. 35, 375–381. https://doi.org/10.1557/mrs2010.570.
He, R.R., Yang, P.D., 2006. Giant piezoresistance effect in silicon nanowires. Nat. Nanotechnol. 1, 42–46.
Hosseinian, E., Pierron, O.N., 2013. Quantitative in situ TEM tensile fatigue testing on nanocrystalline metallic ultrathin films. Nanoscale 5, 12532–12541. https://doi.org/10.1039/c3nr04035f.
Jiang, T., Zhu, Y., 2015. Measuring graphene adhesion using atomic force microscopy with a microsphere tip. Nanoscale 7, 10760–10766. https://doi.org/10.1039/C5NR02480C.
Jiang, T., Huang, R., Zhu, Y., 2014. Interfacial sliding and buckling of monolayer graphene on a stretchable substrate. Adv. Funct. Mater. 24, 396–402. https://doi.org/10.1002/adfm.201301999.
Kang, W., Saif, M.T.A., 2011. A novel SiC MEMS apparatus for in situ uniaxial testing of micro/nanomaterials at high temperature. J. Micromech. Microeng. 21. 105017. https://doi.org/10.1088/0960-1317/21/10/105017.
Kang, W., Saif, M.T.A., 2013. In situ study of size and temperature dependent brittle-to-ductile transition in single crystal silicon. Adv. Funct. Mater. 23, 713–719. https://doi.org/10.1002/adfm.201201992.
Kang, W., Han, J.H., Saif, M.T.A., 2010. A novel method for in situ uniaxial tests at the micro/nano scale – Part II: experiment. Microelectromech. Syst. J. 19.https://doi.org/10.1109/JMEMS.2010.2076782.
Kang, W., Merrill, M., Wheeler, J.M., 2017. In situ thermomechanical testing methods for micro/nano-scale materials. Nanoscale 9, 2666–2688. https://doi.org/10.1039/C6NR07330A.
Kim, J.S., Lagrange, T., Reed, B.W., *et al.*, 2008. Imaging of transient structures using nanosecond in situ TEM. Science 321, 1472–1475. https://doi.org/10.1126/science.1161517.
Kim, K.S., Zhao, Y., Jang, H., *et al.*, 2009. Large-scale pattern growth of graphene films for stretchable transparent electrodes. Nature 457, 706–710. https://doi.org/10.1038/nature07719.
Kiuchi, M., Matsui, S., Isono, Y., 2007. Mechanical characteristics of FIB deposited carbon nanowires using an electrostatic actuated nano tensile testing device. J. Microelectromech. Syst. 16, 191–201.
Kiuchi, M., Matsui, S., Isono, Y., 2008. The piezoresistance effect of FIB-deposited carbon nanowires under severe strain. J. Micromech. Microeng. 18. 065011. https://doi.org/10.1088/0960-1317/18/6/065011.
Li, C., Cheng, G., Wang, H., Zhu, Y., 2020a. Microelectromechanical systems for nanomechanical testing: Displacement- and force-controlled tensile testing with feedback control. Exp. Mech. 60, 1005–1015. https://doi.org/10.1007/s11340-020-00619-z.
Li, C., Zhang, D., Cheng, G., Zhu, Y., 2020b. Microelectromechanical systems for nanomechanical testing: Electrostatic actuation and capacitive sensing for high-strain-rate testing. Exp. Mech. 60, 329–343. https://doi.org/10.1007/S11340-019-00565-5/FIGURES/15.
Liang, H.Y., Upmanyu, M., Huang, H.C., 2005. Size-dependent elasticity of nanowires: Nonlinear effects. Phys. Rev. B 71. 241403.
Liebig, J.P., Göken, M., Richter, G., *et al.*, 2016. A flexible method for the preparation of thin film samples for in situ TEM characterization combining shadow-FIB milling and electron-beam-assisted etching. Ultramicroscopy 171, 82–88. https://doi.org/10.1016/J.ULTRAMIC.2016.09.004.
Lipomi, D.J., Vosgueritchian, M., Tee, B.C.-K., *et al.*, 2011. Skin-like pressure and strain sensors based on transparent elastic films of carbon nanotubes. Nat. Nanotechnol. 6, 788–792. https://doi.org/10.1038/nnano.2011.184.
Liu, X.H., Wang, J.W., Huang, S., *et al.*, 2012. In situ atomic-scale imaging of electrochemical lithiation in silicon. Nat. Nanotechnol. 7, 749–756. https://doi.org/10.1038/nnano.2012.170.
Locascio, M., Peng, B., Zapol, P., *et al.*, 2009. Tailoring the load carrying capacity of MWCNTs through inter-shell atomic bridging. Exp. Mech. 49, 169–182.
Loh, O., Espinosa, H.D., 2012. Nanoelectromechanical contact switches. Nat. Nanotechnol. 7, 283–295.
Lott, C.D., McLain, T.W., Harb, J.N., Howell, L.L., 2002. Modeling the thermal behavior of a surface-micromachined linear-displacement thermomechanical microactuator. Sens. Actuators A Phys. 101, 239–250.
Lu, Y., Song, J., Huang, J.Y., Lou, J., 2011b. Fracture of Sub-20nm ultrathin gold nanowires. Adv. Funct. Mater. 21, 3982–3989. https://doi.org/10.1002/adfm.201101224.
Lu, Y., Peng, C., Ganesan, Y., Huang, J.Y., Lou, J., 2011a. Quantitative in situ TEM tensile testing of an individual nickel nanowire. Nanotechnology 22. 355702. https://doi.org/10.1088/0957-4484/22/35/355702.
McAlpine, M.C., Friedman, R.S., Jin, S., *et al.*, 2003. High-performance nanowire electronics and photonics on glass and plastic substrates. Nano Lett. 3, 1531–1535.
Messenger, R.K., Aten, Q.T., McLain, T.W., Howell, L.L., 2009. Piezoresistive feedback control of a MEMS thermal actuator. J. Microelectromech. Syst. 18, 1267–1278.
Minor, A.M., Dehm, G., 2019. Advances in In situ nanomechanical testing. MRS Bull. 44, 438–442. https://doi.org/10.1557/MRS.2019.127.
Murphy, K.F., Chen, L.Y., Gianola, D.S., 2013. Effect of organometallic clamp properties on the apparent diversity of tensile response of nanowires. Nanotechnology 24. 235704. https://doi.org/10.1088/0957-4484/24/23/235704.
Murphy, K.F., Piccione, B., Zanjani, M.B., Lukes, J.R., Gianola, D.S., 2014. Strain- and defect-mediated thermal conductivity in silicon nanowires. Nano Lett. 14, 3785–3792. https://doi.org/10.1021/nl500840d.
Na, S.R., Wang, X., Piner, R.D., *et al.*, 2016. Cracking of polycrystalline graphene on copper under tension. ACS Nano 10, 9616–9625. https://doi.org/10.1021/ACSNANO.6B05101/ASSET/IMAGES/NN-2016-05101R_M004.GIF.
Naraghi, M., Chasiotis, I., Kahn, H., Wen, Y., Dzenis, Y., 2007a. Novel method for mechanical characterization of polymeric nanofibers. Rev. Sci. Instrum. 78.
Naraghi, M., Chasiotis, I., Kahn, H., Wen, Y.K., Dzenis, Y., 2007b. Mechanical deformation and failure of electrospun polyacrylonitrile nanofibers as a function of strain rate. Appl. Phys. Lett. 91. 151901.
Naraghi, M., Ozkan, T., Chasiotis, I., Hazra, S.S., de Boer, M.P., 2010. MEMS platform for on-chip nanomechanical experiments with strong and highly ductile nanofibers. J. Micromech. Microeng. 20. 125022. https://doi.org/10.1088/0960-1317/20/12/125022.
Narayanan, S., Cheng, G., Zeng, Z., Zhu, Y., Zhu, T., 2015. Strain hardening and size effect in five-fold twinned Ag nanowires. Nano Lett. 15, 4037–4044.
Oh, Y., Cyrankowski, E., Shan, Z.W., Asif, S.A.S., 2010. Micro/Nano-mechanical Test System Employing Tensile Test Holder with Push-to-Pull Transformer. 20100095780.
Ophus, C., 2019. Four-Dimensional scanning transmission electron microscopy (4D-STEM): From scanning nanodiffraction to ptychography and beyond. Microsc. Microanal. 25, 563–582. https://doi.org/10.1017/S1431927619000497.
Ouyang, J., Zhu, Y., 2012. Z-Shaped MEMS thermal actuators: Piezoresistive self-sensing and preliminary results for feedback control. J. Microelectromech. Syst. 21, 596–604. https://doi.org/10.1109/JMEMS.2012.2189361.
Ozkan, T., Naraghi, M., Chasiotis, I., 2010. Mechanical properties of vapor grown carbon nanofibers. Carbon 48, 239–244. https://doi.org/10.1016/j.carbon.2009.09.011.
Pant, B., Allen, B.L., Zhu, T., Gall, K., Pierron, O.N., 2011. A versatile microelectromechanical system for nanomechanical testing. Appl. Phys. Lett. 98. 053506. https://doi.org/10.1063/1.3553195.
Pant, B., Choi, S., Baumert, E.K., *et al.*, 2012. MEMS-based nanomechanics: Influence of MEMS design on test temperature. Exp. Mech. 52, 607–617. https://doi.org/10.1007/s11340-011-9526-8.
Pantano, M.F., Bernal, R.A., Pagnotta, L., Espinosa, H.D., 2014. Multiphysics design and implementation of a microsystem for displacement-controlled tensile testing of nanomaterials. Meccanica 50, 549–560. https://doi.org/10.1007/s11012-014-9950-9.

Papageorgiou, D.G., Kinloch, I.A., Young, R.J., 2017. Mechanical properties of graphene and graphene-based nanocomposites. Prog. Mater. Sci. 90, 75–127. https://doi.org/10.1016/J.PMATSCI.2017.07.004.
Park, H.S., Zimmerman, J.A., 2005. Modeling inelasticity and failure in gold nanowires. Phys. Rev. B 72. 54106.
Peng, B., Locascio, M., Zapol, P., *et al.*, 2008. Measurements of near-ultimate strength for multiwalled carbon nanotubes and irradiation-induced crosslinking improvements. Nat. Nanotechnol. 3, 626–631.
Peng, C., Zhan, Y., Lou, J., 2012. Size-dependent fracture mode transition in copper nanowires. Small 8, 1889–1894. https://doi.org/10.1002/smll.201101911.
Qin, Q., Zhu, Y., 2013. Temperature control in thermal microactuators with applications to in-situ nanomechanical testing. Appl. Phys. Lett. 102. 013101. https://doi.org/10.1063/1.4773359.
Qin, Q., Xu, F., Cao, Y., Ro, P.I., Zhu, Y., 2012. Measuring true young's modulus of a cantilevered nanowire: Effect of clamping on resonance frequency. Small 8, 2571–2576.
Qin, Q., Yin, S., Cheng, G., *et al.*, 2015. Recoverable plasticity in penta-twinned metallic nanowires governed by dislocation nucleation and retraction. Nat. Commun. 6, 5983. https://doi.org/10.1038/ncomms6983.
Que, L., Park, J.-S., Gianchandani, Y.B., 2001. Bent-beam electrothermal actuators-Part I: Single beam and cascaded devices. J. Microelectromech. Syst. 10, 247–254. https://doi.org/10.1109/84.925771.
Rajagopalan, J., Han, J.H., Saif, M.T.A., 2007. Plastic deformation recovery in freestanding nanocrystalline aluminum and gold thin films. Science 315, 1831–1834.
Ramachandramoorthy, R., Gao, W., Bernal, R., Espinosa, H., 2016. High strain rate tensile testing of silver nanowires: Rate-dependent brittle-to-ductile transition. Nano Lett. 16, 255–263. https://doi.org/10.1021/acs.nanolett.5b03630.
Ramachandramoorthy, R., Wang, Y., Aghaei, A., *et al.*, 2017. Reliability of single crystal silver nanowire-based systems: Stress assisted instabilities. ACS Nano 11, 4768–4776. https://doi.org/10.1021/acsnano.7b01075.
Richter, G., Hillerich, K., Gianola, D.S., *et al.*, 2009. Ultra high strength single crystalline nanowhiskers grown by physical vapor deposition. Nano Lett. 9, 3048–3052.
Robertson, I.M., Ferreira, P.J., Dehm, G., Hull, R., Stach, E.A., 2008. Visualizing the behavior of dislocations—seeing is believing. MRS Bull. 33, 122–131.
Robertson, I.M., Schuh, C.A., Vetrano, J.S., *et al.*, 2011. Towards an integrated materials characterization toolbox. J. Mater. Res. 26, 1341–1383.
Ryu, S.Y., Xiao, J.L., Il Park, W., *et al.*, 2009. Lateral buckling mechanics in silicon nanowires on elastomeric substrates. Nano Lett. 9, 3214–3219.
Saif, M.T.A., MacDonald, N.C., 1996. A millinewton microloading device. Sens. Actuators A Phys. 52, 65–75.
Samuel, B.A., Haque, M.A., Yi, B., Rajagopalan, R., Foley, H.C., 2007. Mechanical testing of pyrolysed poly-furfuryl alcohol nanofibres. Nanotechnology 18. 115704. https://doi.org/10.1088/0957-4484/18/11/115704.
Shim, H.W., Huang, H.C., 2007. Three-stage transition during silicon carbide nanowire growth. Appl. Phys. Lett. 90.
Shim, H.W., Zhou, L.G., Huang, H., Cale, T.S., 2005. Nanoplate elasticity under surface reconstruction. Appl. Phys. Lett. 86. 151912.
Shin, J., Richter, G., Gianola, D.S., 2020. Suppressing instabilities in defect-scarce nanowires by controlling the energy release rate during incipient plasticity. Mater. Des. 189. 108460. https://doi.org/10.1016/j.matdes.2019.108460.
Signorello, G., Karg, S., Björk, M.T., Gotsmann, B., Riel, H., 2013. Tuning the light emission from GaAs nanowires over 290 meV with uniaxial strain. Nano Lett. 13, 917–924. https://doi.org/10.1021/nl303694c.
Signorello, G., Lörtscher, E., Khomyakov, P.a, *et al.*, 2014. Inducing a direct-to-pseudodirect bandgap transition in wurtzite GaAs nanowires with uniaxial stress. Nat. Commun. 5, 3655. https://doi.org/10.1038/ncomms4655.
Sim, G.-D., Park, J.-H., Uchic, M.D., *et al.*, 2013. An apparatus for performing microtensile tests at elevated temperatures inside a scanning electron microscope. Acta Mater. 61, 7500–7510.
Spolenak, R., Ludwig, W., Buffiere, J.Y., Michler, J., 2010. In Situ elastic strain measurements—diffraction and spectroscopy. MRS Bull. 35, 368–374.
Steighner, M.S., Snedeker, L.P., Boyce, B.L., *et al.*, 2011. Dependence on diameter and growth direction of apparent strain to failure of Si nanowires. J. Appl. Phys. 109.
Sun, L., Kim, D.H., Oh, K.H., Agarwal, R., 2013. Strain-induced large exciton energy shifts in buckled CdS nanowires. Nano Lett. 13, 3836–3842. https://doi.org/10.1021/nl401860f.
Sun, Y., Xia, Y., 2002. Large-scale synthesis of uniform silver nanowires through a soft, self-seeding, polyol process. Adv. Mater. 14.
Tang, D.-M., Ren, C.-L., Wang, M.-S., *et al.*, 2012. Mechanical properties of Si nanowires as revealed by in situ transmission electron microscopy and molecular dynamics simulations. Nano Lett. 12, 1898–1904. https://doi.org/10.1021/nl204282y.
Tao, W., Cao, P., Park, H.S., 2018. Atomistic simulation of the rate-dependent ductile-to-brittle failure transition in bicrystalline metal nanowires. Nano Lett. 18, 1296–1304. https://doi.org/10.1021/ACS.NANOLETT.7B04972/SUPPL_FILE/NL7B04972_SI_010.AVI.
Tsuchiya, T., Ura, Y., Sugano, K., Tabata, O., 2012. Electrostatic tensile testing device with nanonewton and nanometer resolution and its application to nanowire testing. J. Microelectromech. Syst. 21, 523–529.
Tsuchiya, T., Jomori, T., Ura, Y., Sugano, K., Tabata, O., 2008. Fabrication of free-standing fullerene nanowire using direct electron beam writing and sacrificial dry etching. In: Proceedings of the 2008 IEEE 21st International Conference on Micro Electro Mechanical Systems, pp. 689–692. Available at: https://doi.org/10.1109/MEMSYS.2008.4443750
Wang, J., Sansoz, F., Huang, J., *et al.*, 2013. Near-ideal theoretical strength in gold nanowires containing angstrom scale twins. Nat. Commun. 4, 1742. https://doi.org/10.1038/ncomms2768.
Wang, J., Lu, C., Wang, Q., *et al.*, 2012. Influence of microstructures on mechanical behaviours of SiC nanowires: A molecular dynamics study. Nanotechnology 23. 025703. https://doi.org/10.1088/0957-4484/23/2/025703.
Wang, Z.L., Song, J.H., 2006. Piezoelectric nanogenerators based on zinc oxide nanowire arrays. Science 312, 242–246.
Weinberger, C.R., Cai, W., 2012. Plasticity of metal nanowires. J. Mater. Chem. 22, 3277–3292. https://doi.org/10.1039/c2jm13682a.
Wu, Y., Cui, Y., Huynh, L., *et al.*, 2004. Controlled growth and structures of molecular-scale silicon nanowires. Nano Lett. 4, 433–436.
Xu, F., Lu, W., Zhu, Y., 2011. Controlled 3D buckling of silicon nanowires for stretchable electronics. ACS Nano 5, 672–678.
Xu, F., Qin, Q.Q., Mishra, A., Gu, Y., Zhu, Y., 2010. Mechanical properties of ZnO nanowires under different loading modes. Nano Res. 3, 271–280.
Yan, X., Sharma, P., 2016. Time-scaling in atomistics and the rate-dependent mechanical behavior of nanostructures. Nano Lett. 16, 3487–3492. https://doi.org/10.1021/ACS.NANOLETT.6B00117/SUPPL_FILE/NL6B00117_SI_008.AVI.
Yan, X., Cao, P., Tao, W., Sharma, P., Park, H.S., 2016. Atomistic modeling at experimental strain rates and timescales. J. Phys. D Appl. Phys. 49. 493002. https://doi.org/10.1088/0022-3727/49/49/493002.
Yang, Y., Song, Z., Lu, G., *et al.*, 2021. Intrinsic toughening and stable crack propagation in hexagonal boron nitride. Nature 594, 57–61. https://doi.org/10.1038/s41586-021-03488-1. 5947861.
Yao, S., Zhu, Y., 2015. Nanomaterial-enabled stretchable conductors: Strategies, materials and devices. Adv. Mater. 27, 1480–1511. https://doi.org/10.1002/adma.201404446.
Yashinski, M.S., Muhlstein, C.L., 2013. The role of deposited layers in the nonlinear constitutive behavior of Si nanowires. J. Appl. Phys. 114. 193507. https://doi.org/10.1063/1.4828714.
Yilmaz, M., Kysar, J.W., 2013. Monolithic integration of nanoscale tensile specimens and MEMS structures. Nanotechnology 24. 165502.
Yin, S., Cheng, G., Chang, T.H., *et al.*, 2019a. Hydrogen embrittlement in metallic nanowires. Nat. Commun. 10.https://doi.org/10.1038/s41467-019-10035-0. 2004.
Yin, S., Cheng, G., Richter, G., Gao, H., Zhu, Y., 2019b. Transition of deformation mechanisms in single-crystalline metallic nanowires. ACS Nano 13, 9082–9090. https://doi.org/10.1021/acsnano.9b03311.
Zhang, D., Breguet, J.-M., Clavel, R., *et al.*, 2009a. In situ tensile testing of individual Co nanowires inside a scanning electron microscope. Nanotechnology 20. 365706. https://doi.org/10.1088/0957-4484/20/36/365706.
Zhang, D., Breguet, J.-M., Clavel, R., *et al.*, 2010. In Situ electron microscopy mechanical testing of silicon nanowires using electrostatically actuated tensile stages. J. Microelectromech. Syst. 19, 663–674. https://doi.org/10.1109/JMEMS.2010.2044746.

Zhang, D.F., Drissen, W., Breguet, J.M., Clavel, R., Michler, J., 2009b. A high-sensitivity and quasi-linear capacitive sensor for nanomechanical testing applications. J. Micromech. Microeng. 19. 075003.
Zhang, P., Ma, L., Fan, F., *et al*., 2014. Fracture toughness of graphene. Nat. Commun. 51 (5), 1–7. https://doi.org/10.1038/ncomms4782.
Zhang, Y., Liu, X., Ru, C., *et al*., 2011. Piezoresistivity characterization of synthetic silicon nanowires using a MEMS device. J. Microelectromech. Syst. 20, 959–967.
Zhang, Y.F., Han, X.D., Zheng, K., *et al*., 2007. Direct observation of super-plasticity of beta-SiC nanowires at low temperature. Adv. Funct. Mater. 17, 3435–3440.
Zhang, H., Tersoff, J., Xu, S., *et al*., 2016. Approaching the ideal elastic strain limit in silicon nanowires. Sci. Adv. 2.e1501382.
Zheng, H., Cao, A., Weinberger, C.R., *et al*., 2010. Discrete plasticity in sub-10-nm-sized gold crystals. Nat. Commun. 1, 144. https://doi.org/10.1038/ncomms1149.
Zhou, L.G., Huang, H.C., 2004. Are surfaces elastically softer or stiffer? Appl. Phys. Lett. 84, 1940–1942.
Zhu, T., Li, J., Samanta, A., Leach, A., Gall, K., 2008. Temperature and strain-rate dependence of surface dislocation nucleation. Phys. Rev. Lett. 100. 25502.
Zhu, Y., 2016. In Situ nanomechanical testing of crystalline nanowires in electron microscopes. JOM 68, 84–93. https://doi.org/10.1007/s11837-015-1614-2.
Zhu, Y., Espinosa, H.D., 2005. An electromechanical material testing system for in situ electron microscopy and applications. Proc. Natl. Acad. Sci. USA 102, 14503–14508.
Zhu, Y., Chang, T.-H., 2015. A review of microelectromechanical systems for nanoscale mechanical characterization. J. Micromech. Microeng. 25. 093001. https://doi.org/10.1088/0960-1317/25/9/093001.
Zhu, Y., Moldovan, N., Espinosa, H.D., 2005. A microelectromechanical load sensor for in situ electron and x-ray microscopy tensile testing of nanostructures. Appl. Phys. Lett. 86. 13506.
Zhu, Y., Corigliano, A., Espinosa, H.D., 2006. A thermal actuator for nanoscale in situ microscopy testing: Design and characterization. J. Micromech. Microeng. 16, 242–253.
Zhu, Y., Ke, C., Espinosa, H.D., 2007. Experimental techniques for the mechanical characterization of one-dimensional nanostructures. Exp. Mech. 47, 7–24.
Zhu, Y., Xu, F., Qin, Q., Fung, W.Y., Lu, W., 2009. Mechanical properties of vapor-liquid-solid synthesized silicon nanowires. Nano Lett. 9, 3934–3939. https://doi.org/10.1021/nl902132w.
Zhu, Y., Qin, Q.Q., Xu, F., *et al*., 2012. Size effects on elasticity, yielding and fracture of silver nanowires: In situ experiments. Phys. Rev. B 85. 45443.